

# Modeling spectral evolution of PWNe inside SNRs

N. Bucciantini<sup>1,2\*</sup>, J. Arons<sup>2,3</sup>, E. Amato<sup>4</sup>

<sup>1</sup>*NORDITA, Roslagstullsbacken 23, 106 91 Stockholm, Sweden*

<sup>2</sup>*Astronomy Department and Theoretical Astrophysics Center, University of California, Berkeley, 601 Campbell Hall, Berkeley CA, 94720*

<sup>3</sup>*Department of Physics, University of California, Berkeley, Le Conte Hall, Berkeley, CA 94720*

<sup>4</sup>*INAF, Osservatorio di Arcetri, Firenze, L.go Fermi 5, 50125, Firenze, Italy*

Accepted . Received ; in original form

## ABSTRACT

We present a new model for the spectral evolution of Pulsar Wind Nebulae inside Supernova Remnants. The model couples the long-term dynamics of these systems, as derived in the 1-D approximation, with a 1-zone description of the spectral evolution of the emitting plasma. Our goal is to provide a simplified theoretical description that can be used as a tool to put constraints on unknown properties of PWN-SNR systems: a piece of work that is preliminary to any more accurate and sophisticated modeling. In the present paper we apply the newly developed model to a few objects of different ages and luminosities. We find that an injection spectrum in the form of a broken-power law gives a satisfactory description of the emission for all the systems we consider. More surprisingly, we also find that the intrinsic spectral break turns out to be at a similar energy for all sources, in spite of the differences mentioned above. We discuss the implications of our findings on the workings of pulsar magnetospheres, pair multiplicity and on the particle acceleration mechanism(s) that might be at work at the pulsar wind termination shock.

**Key words:** supernova remnants; pulsars: general; stars: winds, outflows; radiation mechanisms: non-thermal

## 1 INTRODUCTION

Pulsars (PSRs) are known to release most of their rotational energy in the form of a relativistic magnetized wind, whose particle component is mostly made of electron-positron pairs, with, possibly, a minority of ions, while the magnetic field is almost purely toroidal far away from the light cylinder (e.g. Goldreich & Julian (1969)). The wind is initially confined by the slowly expanding Supernova Remnant (SNR), which leads to the formation of a termination shock at some distance from the pulsar, and of a bubble of relativistically hot fluid beyond it. This is the so-called Pulsar Wind Nebula (PWN), that shines through synchrotron and Inverse-Compton emission from radio wavelengths up to  $\gamma$ -rays.

The typical energy that a pulsar injects into the PWN during its entire lifetime is about  $10^{-2}$  of the typical energy of the SN explosion ( $10^{51}$  erg). Therefore, the presence of an energetic PSR, has little effect on the global evolution of the SNR. In contrast, the evolution of the PWN strongly depends on its interaction with the SNR (see Sec. 3).

Modeling of the evolution and dynamical properties of PWN-SNR systems has much improved since the pioneering one-dimensional analytical works by Rees & Gunn (1974) and Kennel & Coroniti (1984a). In recent years, the impressive advances in X-ray observations, due to *CHANDRA* and *XMM-Newton*, have led to a renewed interest in these objects. A major effort has been devoted to explaining the observed X-ray properties of the Crab Nebula and other young systems through multi-dimensional time-dependent approaches to their dynamics (Komissarov & Lyubarsky 2004; Del Zanna et al. 2004, 2006). Several authors (Blondin et al. 2001; van der Swaluw et al. 2001; Bucciantini et al. 2004b; de Jager et al. 2008) have presented numerical evolutionary models, extended to advanced ages (typically up to  $\sim 10^5$  yr), and to the case of fast moving pulsars (van der Swaluw et al. 2004), but in fact, fully multidimensional models are still lacking in these cases. The reason for this is that detailed modeling of older systems is far more difficult than for the young ones: the latter are brighter, hence providing us with high quality multi-frequency data, and are often better constrained in terms of the most relevant physical quantities, such as age, distance and pulsar energetics.

\* E-mail: nbucciantini@nordita.org

The overall evolution of old objects is much more complex than the smooth expansion appropriate to describe young systems. In general, even within the most simplistic approach, the long-term evolution of a PWN-SNR system depends on many parameters: the SN energy, the mass of the ejecta, their density structure, the density of the ISM, the PSR luminosity, its spin-down history (Bucciantini et al. 2004b). A model for particle injection and spectral evolution must be added to all of this, if the aim is that of deriving information from direct comparison with observations. At present, multi-dimensional numerical simulations are not suitable to properly investigate the large parameter space that older systems may span.

The situation is actually delicate also for many young systems. Indeed, accurate multidimensional results, including emission maps to be directly compared with observations, have been so far presented only for the Crab Nebula. But this is a very special object, for which measurements are available through almost the entire electromagnetic spectrum and almost all the aforementioned parameters are known, including the age and the pulsar rotational history (initial spin frequency and braking index). For other young systems, like 3C58 or MSH 15-52, the quantity and quality of information available is much poorer than in the case of Crab and simplified evolutionary models are again the only possible tool for investigation, at least for a start.

Models for the evolution of the emission properties of PWNe have a long history, from the work by Pacini & Salvati (1973), to the most recent developments by de Jager et al. (2008), and Gelfand et al. (2009). These later works have attempted at taking into account both the dynamics of PWN-SNR systems, as derived from accurate numerical simulations, and the spectral evolution of the particle distribution function. In particular, the work by Gelfand et al. (2009) is exemplary for showing the richness of behaviors that is found even within the one-zone treatment, and the degree of complexity that one can investigate using simple tools.

While constraining the unknown parameters is preliminary to detailed multi-dimensional modeling of the systems, which can only sample a much more limited range of parameters, the question arises of how strong and reliable the results obtained with a 1-zone approach are. The recent success of 2-d models of PWNe at reproducing so many of the observed features has interesting consequences in this respect, in that it lends support to the 1-zone description over the 1-dimensional approximation. The latter inevitably leads to onion-like structures (Kennel & Coroniti 1984b), where particles injected at earlier times are located at larger radii, with a one-to-one correspondence between the properties of the particle distribution function and the distance from the central PSR. Comparison of multidimensional models with observations has shown that such ordered structure is not what is realized in PWNe, where an overall turbulent flow is injected at the termination shock and survives through most of the nebular extent (Camus et al. 2009). For the typical flow times, that are much smaller than the PWN age, this turbulent flow-structure leads to efficient mixing, which is what a 1-zone description is based on. This also finds some direct hints from observations where detailed data are available, as in the case of the Crab Nebula: the remarkable homogeneity of radio spectral index across the nebula,

and the extent of the X-ray emitting region which exceeds the predictions of any simple 1-dimensional flow model in the absence of particle diffusion far more efficient than the Bohm rate (Amato et al. 2000).

In the following we present a simplified evolutionary model, similar in spirit to the work by Gelfand et al. (2009). Our approach combines analytical results and numerical simulations for the description of the dynamics of the PWN-SNR system and the evolution of the particle distribution function within the PWN: the key features of the interaction between a PWN and the surrounding SNR are adequately reproduced during different evolutionary stages. The model is here applied to a few systems of various ages, both young and older ones with the aim of showing how this kind of modeling can help the extraction of information on the system properties from multi-wavelength observations: we try to clarify how these properties depend on the different parameters, also discussing potential degeneracies and the observations that would best serve to disentangle them.

Special attention is devoted to the particularly interesting and difficult task of constraining the particle injection in PWNe. The relevance of this issue in terms of pulsar physics and shock acceleration physics deserves a somewhat extended discussion, which will be the topic of next section (Sec. 2).

The rest of the paper is organized as follows. Sec. 3, Sec. 4 and Sec. 5 describe, respectively, how the nebular evolution is implemented in our model, the scheme we adopt to follow the evolution of the particle distribution function and the emission model. In Sec. 6 we show the application of our model to several objects, and, finally, in Sec. 7 we discuss the implications of our findings.

## 2 PARTICLE INJECTION IN PWNE

Forty years of research on Rotation Powered Pulsars have led to a conundrum: observations of young Pulsar Wind Nebulae (PWNe) have clearly established large particle injection rates into the nebulae, well in excess of the electrodynamic minimum suggested by Goldreich & Julian (1969). The latter corresponds to:

$$\begin{aligned}\dot{N}_R &= \frac{c\Phi}{e} = \left(\frac{cI\Omega\dot{\Omega}}{e^2}\right)^{1/2} \\ &= 7.6 \times 10^{33} \left(\frac{I_{45}}{P_{33}^3} \frac{\dot{P}}{4 \times 10^{-13}}\right)^{1/2} \text{ s}^{-1},\end{aligned}\quad (1)$$

where  $\Phi = \sqrt{L/c}$  is the magnetospheric potential,  $L = I\Omega\dot{\Omega}$  is the spin down luminosity, with  $I$  the neutron star's moment of inertia ( $I_{45} = I/10^{45} \text{ g cm}^2$ ),  $\Omega = 2\pi/P$  the stellar angular velocity and  $P$  the rotation period ( $P_{33} = P/33 \text{ msec}$ ). The simplest estimates (Rees & Gunn 1974; Kennel & Coroniti 1984a) show that X-ray emitting PWNe (Kargaltsev & Pavlov 2008) with synchrotron cooling times of the X-ray emitting particles well less than the nebular ages have electron (and positron) injection rates much larger than shown in Eq. (1): values reported in the literature for the multiplicity  $\kappa = \dot{N}/\dot{N}_R$  are typically  $\sim 10^4$ , based on analysis of the X-ray emission, a result consistent with theoretically derived pair creation rates for the young, high

voltage pulsars which have been subjected to such analysis [*e.g.* Kennel & Coroniti (1984a); Gaensler et al. (2002); Hibschan & Arons (2001)]. Indeed, the fact that the inferred injection rates are this large is one of the major pillars of support for the theoretical conclusion that pulsars have substantial outflows of  $e^\pm$ , this being the only known means through which such cool objects can have winds denser than the electrodynamic minimum.

Such high density flows with  $\kappa \gg 1$  support the use of the force-free limit of MHD theory in modeling the torques on rotation powered neutron stars (Kalapotharakos & Contopoulos 2009; Spitkovsky 2006). As already mentioned, MHD theory has been quite successful in modeling the multidimensional dynamics and appearance of young PWNe (Komissarov & Lyubarsky 2004; Del Zanna et al. 2004, 2006; Volpi et al. 2008). Such models confirm the early inference (Rees & Gunn 1974; Kennel & Coroniti 1984a) that the system behaves as if just upstream of the pulsar wind termination shock (TS) the plasma has low magnetization  $\sigma_w \equiv (B^2/8\pi\gamma_w n_\pm m_\pm c^2) \ll 1$  ( $n_\pm$  is the number density of pairs, the particle density is  $2n_\pm$ ): typically, the average of  $\sigma_w$  in latitude with respect to the rotation axis is<sup>1</sup>  $\sim 0.02$ .

The nebular dynamics in the MHD model is insensitive to the specific value of the upstream 4-velocity  $u_w = c\beta_w\gamma_w$ , as long as  $\gamma_w \gg 1$ . By applying their 1D MHD model to the optical and harder photon emission in the Crab, Kennel & Coroniti (1984b) inferred  $\gamma_w \approx 10^{6.5}$ , with  $\sigma_w \approx 0.005$ . More modern models (Del Zanna et al. 2006; Volpi et al. 2008) require latitude averaged  $\sigma_w$  to be somewhat larger (so that magnetic hoop stress can create the jet component of the torus-jet structure), while account of the high energy synchrotron emission requires particle spectra at the TS with parameters similar to the 1D Kennel and Coroniti model: again  $\gamma_w \sim 10^6$ , although this is not explicitly stated since the distribution functions were not tied to the specifics of the MHD flow.

If the apparent low value of  $\sigma_w$  means that the wind just upstream of the TS really is weakly magnetized,  $\sigma_w$  and  $\gamma_w$  are closely tied to the pair multiplicity  $\kappa_\pm = \kappa/2$ , since when  $\sigma \ll 1$  the wind carries the rotational energy lost from the pulsar in kinetic energy of the flow,  $L = \dot{M}c^2\gamma_w$ . Since  $\dot{M} = 2\kappa_\pm m_\pm \dot{N}_R = 2\kappa_\pm m_\pm c\Phi/e$ , and  $L = c\Phi^2$ , then  $\gamma_w = e\Phi/2m_\pm c^2\kappa_\pm$ . In the case of the Crab Nebula and pulsar,  $\Phi = 4 \times 10^{16}$  V, while extant theoretical models of pair creation, from polar caps, slot gaps or outer gaps (Hibschan & Arons 2001; Cheng 2007; Hirotani 2008; Harding 2004) all yield  $\kappa_\pm \sim 10^4$ , for young pulsars with  $\Phi > 10^{15}$  V. Thus theory also says  $\gamma_w \sim 10^6$  - if one confines one's analysis to the high frequency emission from PWNe, theory and observation appear to be in good accord<sup>2</sup>.

Using the X-ray emitting particles in PWNe, whose synchrotron cooling times are short, takes advantage of such PWNe being calorimeters for the contemporary particle injection rates, which gives the results some independence

from the uncertainties of evolutionary models. However, radio and infrared emitting particles are much more numerous than the X-ray emitting ones, due to the rapid decline of synchrotron emissivity with declining particle energy (Kennel & Coroniti 1984b; Gallant *et al.* 2002). Models of the underlying pulsar must be able to account for *all* the radiating relativistic particles found in the PWNe - the spectral continuity in several systems demonstrated in the results described below suggests the lower energy particles are indeed injected by the pulsar, rather than being accelerated out of the non-relativistic material often found embedded within PWNe. Thus measuring the full relativistic particle content in PWNe is an important experimental input into modeling of pulsars, distinct from the modeling of the energy input into the nebulae. For the latter the force free model (Spitkovsky 2006; Kalapotharakos & Contopoulos 2009) provides the essential description, but unfortunately this is independent of the multiplicity, so long as  $\kappa \gg 1$ .

We study several young PWNe (Crab, 3C58, B1509, Kes75) for which the data can be used to reasonably constrain the pair injection rate - in principle one would like to use nebulae with ages known, and reasonably complete (including near and far infrared and millimeter) spectral energy distributions (SEDs) are required. We show that all these systems have spectral continuity from the radio through the infrared to the X-ray bands, suggesting a single source for the radiating particles is present in each system. We use these full SEDs to derive new estimates for the pair creation multiplicity. We discuss the constraints these results set on PSR pair production gap models - Polar Caps, Slot Gaps, and Outer Gaps - concluding that no existing model adequately explains particle injection rates.

We also discuss alternate hypotheses, that low energy particles are picked up from thermal gas in the nebulae, or are fossils left over from some unnamed acceleration process in the early history of the nebula (Atayan & Aharonian 1996), or represent the effects of a second acceleration mechanism operating at low energy (Gallant *et al.* 2002), such as cyclotron acceleration stimulated by a heavy ion component of the wind (Hoshino et al. 1992; Amato & Arons 2006), or more generally any component with Lorentz factor greater than  $\gamma_w$ . We use the spectral continuity to argue that such a two component model is unlikely, implying some additional piece of physics needs to be added to the shock acceleration model to account for these broken power-laws, in addition to the extra physics needed to account for the total injection rate.

### 3 NEBULAR EVOLUTION

There are three phases of interest in the evolution of a PWN. In this section we briefly describe them and explain how we model each of them.

We consider objects of relatively young age (less than 40,000 yr) with the PSR still inside the SNR, and assume spherical symmetry, neglecting the pulsar proper motion (see van der Swaluw et al. (2004) for a discussion of this point). We also assume, in deriving the PWN evolution, that radiation losses of the particles are negligible. Given the weak dependence of the PWN radius on the PSR lu-

<sup>1</sup> This analysis has been done in full only for the Crab Nebula, however.

<sup>2</sup> We neglect a possible component of heavy ions in the wind's composition (Gallant & Arons 1994; Spitkovsky & Arons 2004): this subject will be discussed later on

minosity, and the fact that radiation losses only affect the particle energy content and not the magnetic energy content, we do expect this to be a good approximation. This allows us to use analytical formulae, and substantially reduce the computational requirements.

### 3.1 SNR evolution

In order to model the evolution of a PWN inside a SNR we first need to solve for the evolution of the SNR itself. An excellent semi-analytic model for the evolution of an SNR without an embedded PWN was provided by Truelove & McKee (1999). Using pressure balance between the shocked ISM downstream of the outer forward shock, and the shocked ejecta beyond the reverse shock, they solve for the evolution of both the outer forward shock and the inner reverse shock from the early ejecta dominated phase (Hamilton & Sarazin 1984) to the later Sedov phase (Ostriker & McKee 1988). It is shown that the evolution can be cast in dimensionless form by using the following characteristic variables:

$$R_{ch} = M_{ej}^{1/3} \rho_o^{-1/3} \quad (2)$$

$$t_{ch} = E_{SN}^{1/2} M_{ej}^{5/6} \rho_o^{-1/3} \quad (3)$$

where  $\rho_o$  is the density of the ISM (assumed to be uniform),  $E_{SN}$  is the kinetic energy of the supernova explosion, whose canonical value is  $10^{51}$  erg, and  $M_{ej}$  is the mass of the ejecta. The only free parameter in the Truelove & McKee model is the mass distribution in the ejecta. Unfortunately, this is not directly constrained by observations, and choices in the literature are mostly based on theoretical assumptions: for example Chevalier (1982) suggested a distribution with an inner plateau and outer steep profile; while Truelove & McKee (1999) focus on the case of self-similar ejecta with a density distribution  $\rho_{ej} \propto r^{-\alpha} t^{\alpha-3}$  and a velocity profile  $v_{ej} \propto r$ . Many recent numerical works on young PWNe have indeed adopted the latter distribution, with great success in reproducing the observations (van der Swaluw et al. 2001; van der Swaluw 2003; Bucciantini et al. 2003, 2004; Del Zanna et al. 2004, 2006).

Once the evolution of the SNR is known, it can be used to constrain the evolution of the PWN.

### 3.2 Free expansion phase

The first phase of the PWN evolution is generally referred to as *free-expansion phase*, and has the PWN expanding inside the cold ejecta. This phase lasts for a few thousand years, until the PWN reaches the reverse shock. In this phase, the evolution of the PWN is independent of the evolution of the SNR shell, because no contact has been established between the two yet. In the case of self-similar ejecta and constant PSR luminosity  $L$  a solution for the radius of the PWN as a function of time has been known for a long time (Chevalier & Fransson 1992; van der Swaluw et al. 2001):

$$R(t) \simeq L^{\frac{1}{5-\alpha}} E_{SN}^{\frac{3+\alpha}{10-2\alpha}} M_{ej}^{-1/2} t^{\frac{6-\alpha}{5-\alpha}}. \quad (4)$$

In the more general case in which the PSR luminosity changes in time according to

$$L(t) = L_o / (1 + t/\tau)^\beta, \quad (5)$$

Bucciantini et al. (2004) have shown that it is possible to find an analytic solution and they provide a series expansion for it, showing that already the first few leading terms of the series provide an excellent approximation. In this work we adopt this approach, that allows us to properly include in our model the spin-down properties of the PSR.

The free expansion phase lasts as long as the radius of the PWN is smaller than the radius of the reverse shock computed using the Truelove & McKee model. Once the PWN reaches the reverse shock, the reverberation phase begins.

### 3.3 Reverberation phase

Once the PWN has reached the SNR reverse shock, it is in contact with the shock heated ejecta. The pressure of the hot ejecta is higher than the pressure of the relativistic material inside the PWN. As a consequence, the PWN expansion halts, and the system starts contracting (van der Swaluw et al. 2001).

An analytic model for this phase is not available, however the evolution can be treated within the so called thin-shell approximation (Giuliani 1982): the evolution of the PWN outer radius is described in terms of the evolution of a thin shell of material enclosing a mass  $M_{sw}$  equal to the mass of ejecta that has been swept up by the PWN up to the beginning of the reverberation phase. This shell is bounded on the inner side by a hot relativistic plasma with pressure  $P_{in}$ , and on the outer side by the shock heated ejecta with pressure  $P_{out}$ :

$$M_{sw} \ddot{R}(t) = 4\pi R(t)^2 (P_{in}(t) - P_{out}(t)). \quad (6)$$

The value of the PWN pressure is computed numerically using energy conservation:

$$P_{in}(t) = P_{in}(t_r) + \frac{1}{4\pi R(t)^4} \int_{t_r}^t L(t) R(t) dt, \quad (7)$$

where  $t_r$  is the time at which the reverberation phase begins. It is less clear what  $P_{out}$  should be. A lower limit is given by the pressure that the shock heated ejecta would have in the absence of a PWN. An upper limit corresponds to the pressure of the Sedov solution. Numerical simulations show that the interaction of the SNR with the PWN leads to additional heating of the ejecta, due to sound waves that are launched inside the SNR during the reverberation phase (see Fig. 3 of Bucciantini et al. (2003)). On the other hand, it takes longer for the SNR to relax to the Sedov solution, while during the first compression the value of  $P_{out}$  is found to be close to about 50% of the Sedov value (Bucciantini et al. 2003). In our model we use this fiducial fudge factor.

In 1D simulations (van der Swaluw et al. 2001) the reverberation phase is characterized by a series of compressions and expansions of the nebula, until the system relaxes to the Sedov-Taylor phase, which is finally established once the PWN reaches pressure equilibrium with the SNR. This behavior, which resembles a damped oscillator, is an artifact of the 1D geometry. In more realistic multidimensional regime (Blondin et al. 2001), the evolution of the PWN during the reverberation phase is subject to strong Rayleigh-Taylor (RT) instabilities and efficient mixing of the relativistic material with the SNR matter. From a dynamical point of view this mixing acts as a viscous term on the evolution of

the nebula, and one might expect, instead of a series of oscillations, an almost complete relaxation to the Sedov-Taylor solution after the first compression.

Of course in the presence of mixing and the related clumpiness, the volume occupied by the relativistic plasma will not be directly related to the radial extent of the nebula. However Eq. 7 will still hold if one interprets  $R(t)$  as an effective radius related to the total volume of the relativistic plasma,  $4\pi R(t)^3/3$ , rather than as the radial extent of the nebula (which in general might be larger because of clumpiness). In 1-zone models this effective volume is also all that matters for computing particle adiabatic losses.

In our model the reverberation phase ends after the first compression, once the PWN pressure reaches the value of the Sedov-solution for the SNR.

### 3.4 Sedov-Taylor phase

Once the pressure inside the PWN reaches the value proper of the Sedov solution corresponding to the SNR forward shock, the Sedov-Taylor phase begins. This usually happens at an age  $\sim 10^4$  yr. By this time, because of spin-down, the PSR luminosity can in general be neglected in the evolution of the system. The speed of the forward shock,  $v_{fs}$ , and the post-shock pressure are both given by the Truelove & McKee (1999) model. The pressure inside the SNR is then assumed to be equal to the central pressure of the Sedov solution  $P_{out} \sim 0.5\rho_0 v_{fs}^2$ .

The nebula evolves according to

$$R(t_s)^4 P_{in}(t_s) = R(t)^4 P_{in}(t) = R(t)^4 P_{out}(t), \quad (8)$$

where  $t_s$  is the time at which the Sedov-Taylor phase begins and, again, the radius  $R(t)$  is related to the total volume of the relativistic plasma rather than to the radial extent of the nebula.

One last comment is in order about the role of RT instabilities. While during the reverberation and Sedov-Taylor phase, re-interpretation of the radius appearing in Eqs. 6, 7 and 8 in terms of effective volume is necessary, during the initial free-expansion phase, RT and mixing are not as important: Bucciantini et al. (2004b) and Jun (1998) have shown that, in general, the radius derived from the 1D solution, is at most 10-15% smaller than the true radial extent of the nebula. We might then conclude that at least for very young objects the 1D radial model provides a reliable estimate both for the radial extent of the nebula and for the volume occupied by the relativistic fluid.

## 4 PARTICLE EVOLUTION

Once the evolution of the nebula is known one can compute the evolution of the particle distribution function.

The energy of a particle is evolved according to

$$\frac{dE(t)}{dt} = -\frac{\dot{R}(t)}{R(t)}E(t) - \frac{4\sigma_T}{3m^2c^3}E^2(t) \left( \frac{B(t)^2}{8\pi} + U(t) \right), \quad (9)$$

where  $B(t)$  and  $U(t)$  are the magnetic field and the background photon energy density in the nebula, respectively,  $\sigma_T$  is the Thompson cross section,  $m$  the particle mass. The magnetic field in the nebula is computed assuming that the ratio of magnetic to total energy in the nebula  $\eta_M$  is constant

in time ( $0 < \eta_M < 1$ ), while the total energy is computed considering the pulsar injection and the adiabatic losses of the 1D model as described in Sec. 3. The background photon energy density includes different contributions: CMB and starlight, which are constant in time, and synchrotron (SYN) emission, which is computed, instead, together with the nebular evolution. We have verified that Inverse Compton (IC) losses are in general negligible with respect to SYN losses, and SYN-IC is important only in young compact objects, where the magnetic field is stronger, and the SYN emissivity higher.

Given a particle injected at time  $t_o$  with energy  $E_o$ , one can solve Eq. 9 to derive the energy  $E(t, t_o, E_o)$  of the particle at time  $t$ . An analytic solution of Eq. 9, is not in general available, neither is its inverse, and the energy evolution has to be computed numerically. Once the evolution of the energy is known, then it is possible to compute the evolution of the particle spectrum according to

$$N(E, t) = \int_E^\infty \dot{N}(E_o, t_o) \frac{\partial t_o}{\partial E}(E, E_o, t) dE_o, \quad (10)$$

where  $\dot{N}(E)$  is the particle injection rate per unit energy interval.

Since no analytic solution is available for Eq. 9, also this equation must be solved numerically. Given the very short synchrotron lifetime of the particles at the high energy end of the spectrum we use a Lagrangian scheme in energy space. The energy space is originally divided into energy bins whose extremes are given by  $E_i(t)$ . These evolve according to Eq. 9. When a bin moves to energies lower than 50 keV, it is removed from the sample. New bins are continuously added at the high energy end of the distribution function, as the old ones evolve to lower energies. The time step is then dictated by the requirement of sufficient energy resolution in the high energy portion of the spectrum.

The total number of particles inside the  $i$ -th bin, at each time, is then computed by integrating numerically the following equation:

$$N_i(E_{i+1/2}(t), t) = N_i(E_{i+1/2}(t_o), t_o) + \int_{t_o}^t dt' \int_{E_i(t')}^{E_{i+1}(t')} dE \dot{N}(E, t'), \quad (11)$$

where  $t_o$  is the initial time at which injection in the bin begins. This approach guarantees conservation of particle number.

In principle the functional form of  $\dot{N}(E, t)$  can be arbitrarily chosen.

For the pairs, we assume a broken power-law. Given that injection is due to the PSR wind, and that the only energy scale available in the wind is the PSR voltage,  $\epsilon_v = e\Phi$ , we have decided to use a scale-free model for a broken power-law:

$$\dot{N}(E, t) = C_o(t) \begin{cases} (E/\epsilon_c)^{-\gamma_1} & \text{for } \epsilon_m < E < \epsilon_c \\ (E/\epsilon_c)^{-\gamma_2} & \text{for } \epsilon_c < E < \epsilon_v \end{cases} \quad (12)$$

where  $\gamma_1 < 2 < \gamma_2$ ,  $\epsilon_c$  is the peak of the injected energy distribution  $E\dot{N}(E, t)$  and  $\epsilon_m$  is the low-energy cutoff, usually found to be small compared to  $\epsilon_c$ . The scale free approximation implies that the ratios  $\nu_e = \epsilon_m/\epsilon_v$  and  $\mu_e = \epsilon_c/\epsilon_v$ , are constant in time.  $\mu_e$  and  $\nu_e$  are free parameters of the model, and their value is obtained from a fit to the data.

Once  $\mu_e$  and  $\nu_e$  are fixed,  $C_0(t)$  is given by energy conservation. We have:

$$\eta_e L(t) = \int_{\epsilon_m}^{\epsilon_v} \dot{N}(E, t) E dE \approx \frac{\gamma_2 - \gamma_1}{(\gamma_2 - 2)(2 - \gamma_1)} C_0(t) \epsilon_c^2 \quad (13)$$

with  $\eta_e$  the fraction of the PSR luminosity injected into pairs. The particle number flux in the wind is

$$\dot{N}(t) = \int_{\epsilon_m}^{\epsilon_v} \dot{N}(E, t) dE \approx \frac{C_0(t) \epsilon_c}{\gamma_1 - 1} \left( \frac{\epsilon_c}{\epsilon_m} \right)^{\gamma_1 - 1}, \quad (14)$$

and the average energy/particle in the spectrum (12) is, for  $\epsilon_m \ll \epsilon_c \ll \epsilon_v$ ,

$$\begin{aligned} \langle E \rangle &= \frac{\eta_e L(t)}{\dot{N}(t)} = \gamma_w m_e c^2 \approx \\ &\approx \frac{(\gamma_2 - \gamma_1)(\gamma_1 - 1)}{(\gamma_2 - 2)(2 - \gamma_1)} \epsilon_c \left( \frac{\epsilon_m}{\epsilon_c} \right)^{\gamma_1 - 1}. \end{aligned} \quad (15)$$

In expression 15, we have identified the average energy/pair in the spectrum with the upstream flow energy/pair, but we have not specifically used the shock jump conditions. This is because, as we will discuss in §7, the distribution (12) implies some additional mechanism for energy redistribution, which may or may not be directly connected to the termination shock. From Eq. 15 it is clear how it is possible to estimate the PSR multiplicity through a fit of the model to the PWN emission.

If the wind is characterized by a single value of the Lorentz factor, then  $\gamma_w m_e c^2 \simeq \epsilon_c$ ,  $\eta_e L(t) = m_e c^2 \gamma_w \dot{N}(t)$ . However, the approximation of a single Lorentz factor might not be correct, in this case the ratio  $\epsilon_m/\epsilon_c$  cannot be a priori determined, but is found from requiring a fit to the entire spectrum. In particular, once an upper limit for  $\epsilon_m$  is derived from fitting the low frequency radio emission, this can be used to infer the particle number flux and estimate the average Lorentz factor.

We consider the possibility that a minority by number of high energy particles in the equatorial return current (either positrons, ions or electrons, depending on return current sign) are part of the PSR wind and carry a fraction  $\eta_p$  of the energy flux. Focusing on the case when ions are the implied particles, one might look for signature of their presence. For simplicity we consider them injected with a mono-energetic spectrum centered at an energy  $\gamma_w m_p c^2$  (equivalent to assuming that they are moving at the same Lorentz factor as the pairs injected at  $\epsilon_c$ ). Ions are affected by different loss mechanisms compared to pairs: while radiation losses are negligible, p-p scattering and diffusion outside the nebula might be important. Following the approach of Amato et al. (2003) we assume that both diffusion and p-p scattering remove particles from the distribution function. Due to these effects the number of ions of energy  $E$  between time  $t$  and  $t + dt$  changes by:

$$N(E(t + dt), t + dt) = N(E(t), t) e^{-dt(1/\tau_{pp} + 1/\tau_{dif})} \quad (16)$$

where  $E(t)$  is given by Eq. 9, and where the characteristic p-p timescale is

$$\tau_{pp} \simeq 5(\sigma_o n_t c)^{-1} \quad (17)$$

with  $\sigma_o = 5 \times 10^{-26} \text{ cm}^2$ , and  $n_t$  the target proton density. While the typical diffusion timescale is

$$\tau_{dif} \simeq \frac{R(t)^2}{r_L c} \quad (18)$$

where  $r_L$  is the ions' Larmor radius.

## 5 EMISSION

There are three channels of non-thermal emission in PWNe. From Radio frequencies to MeV photon energies, the dominant emission process is synchrotron radiation by the accelerated electrons and positrons gyrating in the nebular magnetic field. At higher energies, there are two possible contributions: Inverse Compton (IC) emission by the high energy pairs, and gamma-ray emission from neutral pion decay, following “p-p” scattering between accelerated and target protons.

The synchrotron luminosity is computed using the “monochromatic” approximation. The power per unit frequency emitted by a single particle with energy  $\gamma m_e c^2$  is:

$$S(\nu, \gamma) = \frac{4}{3} \sigma_T c \frac{B^2}{8\pi} \gamma^2 \delta(\nu - \nu_c) \quad (19)$$

where  $\sigma_T$  is the Thompson cross section,  $B$  is the nebular magnetic field, and

$$\nu_c = 0.29 \frac{3e}{4\pi m c} B \gamma^2 \quad (20)$$

is the characteristic emission frequency.

Eq. 19 has then to be integrated over the pair distribution function (see previous section) in order to derive the total nebular synchrotron luminosity at a given frequency.

IC is computed using the full Klein-Nishina cross section (Jones 1968; Blumenthal & Gould 1970) and assuming scattering over three main target photon fields: 1) CMB, modeled as a perfect black-body, with typical temperature 2.75 K; 2) synchrotron emission from the PWN, consistently computed as described above; 3) “galactic background”, which in principle includes both galactic starlight and any local contribution in the optical-IR band. This third term is modeled as a suppressed black-body: both the temperature (in the range of a few hundreds/thousands Kelvin), and the suppression factor (of order  $10^{-10}$ ), are in principle free parameters that can be adjusted. The role of this contribution will be discussed in more detail when dealing with specific objects.

Gamma ray emission from neutral pion decay is computed following Amato et al. (2003). In the scaling regime a mono-energetic proton distribution with energy  $E_p$  leads to the following pion injection spectrum

$$\frac{dN_\pi}{dt dE_\pi} = K_\pi E_\pi^{-1} g_\pi(E_\pi/E_p), \quad (21)$$

where

$$g_\pi(x) = (1 - x)^{3.5} + e^{-18x}/1.34 \quad (22)$$

and the constant  $K_\pi$  is found through the normalization condition:

$$N(E_p) \left( \frac{dE_p}{dt} \right)_\pi = \int_{m_\pi c^2}^{E_p} \frac{dN_\pi}{dt dE_\pi} E_\pi dE_\pi, \quad (23)$$

where  $N(E_p)$  is the number of protons with energy  $E_p$ .

The number of photons emitted per unit time and energy interval is then

$$J(e_\gamma) = 4 \left( \frac{dN_{\pi^0}}{dt dE_{\pi^0}} \right)_{E_{\pi^0}=2e_\gamma}. \quad (24)$$

The total pion emissivity is then computed integrating over the total proton energy distribution. The density of target protons  $n_t$  that enters Eq. 17 is the main unknown: if the protons are well confined within the PWN, then a reasonable assumption would be to use the swept-up ejecta mass; if they can leak out then one should consider the total ejecta mass. A realistic model for proton diffusion in PWN-SNR systems is far beyond the scope of this paper: we keep  $n_t$  as a free parameter and discuss the implications of its assumed value whenever relevant.

## 6 RESULTS

In this section we show the results obtained when applying our model to a few objects of different ages, both young and old. For each object, we will not attempt at obtaining the best possible fit of the data, which in our view would not be very significant given the intrinsic limitations of a one-zone model. In fact, our primary interest is to put some constraints on the unknown parameters and to clarify which observations would be more relevant to improve our understanding of these systems. At the same time we will discuss the limitations of this approach and make clear which part of our results should be considered as really reliable.

### 6.1 The Crab Nebula

The Crab Nebula is the system for which we have the best constraints, both regarding the pulsar injection properties, and the luminosity at different wavelengths. Available data extend from low radio frequencies (Baldwin 1971; Baars 1972), through mm/IR (Mezger et al. 1986; Bandiera et al. 2002), optical/UV radiation (Veron-Cetty & Woltjer 1993; Hennessy et al. 1992), X-rays (Kuiper et al. 2001) and  $\gamma$ -rays from MeV to TeV energies (Aharonian et al. 2004; Albert et al. 2008; Abdo et al. 2010). The source distance is estimated to be 2 kpc, and the nebular volume is  $30 pc^3$  (Hester 2008), corresponding to a spherical radius of about 6  $ly$ . This is the only system for which we know the exact age (950 years). We also have a reliable estimate of the braking index (2.51 implying  $\beta = 2.33$ , Lyne et al. (1993)), which, when combined with the present luminosity  $L \simeq 5 \times 10^{38} \text{ erg s}^{-1}$ , allows us to derive an initial luminosity  $L(0) = 3.5 \times 10^{39} \text{ erg s}^{-1}$ , and a characteristic spin-down timescale  $\tau \simeq 730$  years.

Much more uncertain are the properties of the SNR which should be surrounding the nebula. Several attempts at detecting both the forward and the reverse shock have only provided upper limits. More information can be derived by studying the filamentary network surrounding the PWN and comparing the results with theoretical expectations based on hydrodynamical models of the interaction between the nebula and the surrounding ejecta (Hester et al. 1996; Jun 1998; Bucciantini et al. 2004b). The visible remnant contains at least  $1\text{--}2 M_\odot$  of He-rich line-emitting gas and the PWN expands at a speed of about  $1.5 - 2 \times 10^3 \text{ km s}^{-1}$ . Traditional models for the evolution of the Crab Nebula (Chevalier & Fransson 1992; van der Swaluw et al. 2001; Bucciantini et al. 2003; Del Zanna et al. 2004) have all assumed a flat density profile of the ejecta. Steeper

ejecta ( $\alpha \geq 1$  in Table 1) give a mass in the filamentary network higher than what is observed. Assuming flat ejecta and a canonical SN energy of  $10^{51} \text{ erg}$ , in order to reproduce the proper size of the nebula a mass  $M_{ej} = 9.5 M_\odot$  is needed, very close to the most recent estimate by MacAlpine & Satterfield (2008). The lack of any clearly detected SNR shell prevents any reliable estimate of the ISM density and we simply assume a fiducial value of  $0.1 \text{ cm}^{-3}$ .

The PSR and SNR parameters are listed in Table 1, together with the parameters that describe the particle energy distribution at injection. The low energy spectral index  $\gamma_1$  is fixed according to the radio data, while the high energy index  $\gamma_2$  is chosen in order to minimize the X-ray residuals. We want to stress here that the X-ray emission is concentrated in the central region of the PWN and it is strongly affected by the details of the flow dynamics just downstream of the termination shock (Del Zanna et al. 2004, 2006). It is unrealistic to expect that a simplified one-zone model can provide an accurate description of the high energy spectrum. A one-zone model can at most provide an indication of the best power-law index that can fit the data, but more realistic multidimensional models are necessary to address the emission properties in the X-ray band. Two features are interesting to notice: 1)  $\gamma_2$  is higher than the value 2.23 typical of relativistic Fermi shock acceleration with isotropic scattering in the fluid frame; 2) there are indications that a single power-law cannot reproduce the complete set of X-ray data points.

Several features are present at high energies, but it is not clear if they are intrinsic (a suggestion in this sense has been put forward by Volpi et al. (2008), where they present a multidimensional model of the emission that shows similar features), if they are simply due to calibration issues among different instruments or even for one instruments at different energies, or if they are due to temporal variability of the emission properties (Bucciantini 2008).

The present model can reproduce the synchrotron part of the spectrum within few % accuracy (greater discrepancies being present at high energies as discussed above). At present, our particle distribution function does not include any smooth high-energy cut-off, the reason being the very short lifetime of high energy particles that prevents efficient numerical integration of their evolution. However a good match with the data can be obtained by introducing *a posteriori* an exponential cut-off in the particle energy distribution. This reflects in a cut-off in the emission spectrum at a frequency around  $\sim 10^{22} \text{ Hz}$ . Our model requires that 80% of the pulsar spin-down luminosity goes into accelerated pairs. This does not leave much energy to be carried by higher energy particles (i.e. ions (Amato et al. 2003)). In principle the presence of ions might have observable consequences in the TeV band, however even assuming the remaining 20% of the spin-down energy is all carried by ions, their contribution to the gamma-rays emission turns out to be negligible. On the other hand, if the return current is made by a high energy lepton beam (Arons, in preparation), the radiative consequences of this latter scenario have not been investigated, however, again, they are not expected to give any appreciable contribution to gamma-rays

TeV emission is due to IC scattering by the pairs, for which the main target is the nebular synchrotron emission in this case. We estimate a magnetic field  $B \simeq 200 \mu\text{G}$ ,

**Table 1.** Values of the parameters used in the modeling.

Parameter	Symbol	Crab	3C58	B1509-58	Kes 75
Supernova explosion energy ( $10^{51}$ erg)	$E_{SN}$	1	1	7	2.1
Mass of the ejecta ( $M_{\odot}$ )	$M_{ej}$	9.5	3.2	4.0	16.4
ISM density ( $\text{cm}^{-3}$ )	$\rho_o$	0.1	0.01	0.001	2
Ejecta density index	$\alpha$	0	1	1	0
Initial pulsar luminosity ( $10^{38} \text{erg s}^{-1}$ )	$L_o$	35	0.73	49	1.66
Spin-down time (yr)	$\tau$	730	3280	114	226
Braking index	$\beta$	2.33	2	2.087	2.12
Age (yr)	$t$	950	2100	1570	650
Fraction of $L$ that goes into pairs	$\eta_e$	0.8	0.75	0.7	0.95
Low-energy injection index	$\gamma_1$	1.5	1.2	1.2	1.7
High-energy injection index	$\gamma_2$	2.35	2.82	2.14	2.3
Peak energy ratio	$\mu_e$	$1.54 \times 10^{-5}$	$6.25 \times 10^{-6}$	$3.33 \times 10^{-6}$	$10^{-4}$
Minimum energy ratio	$\nu_e$	$1.1 \times 10^{-8}$	$8.7 \times 10^{-8}$	$2.8 \times 10^{-8}$	$2 \times 10^{-7}$
Break energy (eV)	$\epsilon_c$	$4 \times 10^{11}$	$5 \times 10^{10}$	$1.5 \times 10^{10}$	$4 \times 10^{11}$
Fraction of magnetic energy	$\eta_M$	0.11	0.5	0.53	0.005
Fraction of $L$ that goes into ions	$\eta_p$	0	0	0	0

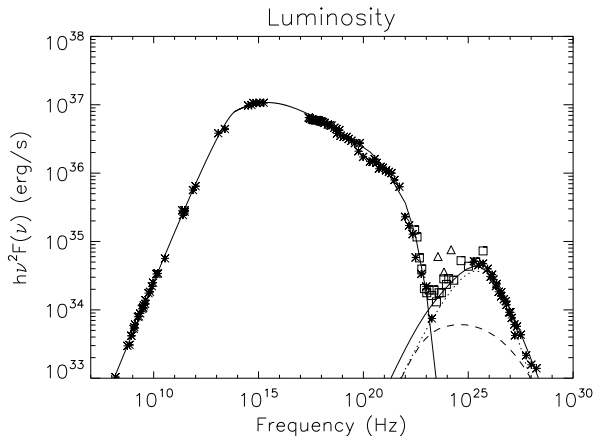


**Figure 1.** The Crab Nebula integrated emission spectrum. Data points are from Baldwin (1971); Baars (1972); Mezger et al. (1986); Bandiera et al. (2002); Veron-Cetty & Woltjer (1993); Hennessy et al. (1992); Kuiper et al. (2001); Aharonian et al. (2004); Albert et al. (2008); Abdo et al. (2010) (triangles are *EGRET* points, squares are *Fermi* points). Solid line is the total luminosity. Dashed line is the IC-CMB, dotted line if the IC-SYN.

slightly lower than previous estimates (Aharonian et al. 2004; Hester 2008). Overall the broad-band spectrum is very well reproduced, with the largest discrepancies limited to the *EGRET* data points around 10 MeV. These points have large uncertainties and are likely affected by calibration issues (Abdo et al. 2009). Indeed recent *Fermi* data (Abdo et al. 2010) are consistent with our model curve.

Baldwin (1971) has shown that the radio power-law spectrum of the Crab Nebula extends down to the ionospheric cut-off at  $\sim 30$  Mhz. One can use this piece of information to derive an upper limit on the minimum particle energy at injection. In order for the radio spectrum to extend to those energies as an uninterrupted power-law, we need to assume  $\epsilon_m/\epsilon_c < 7 \times 10^{-4}$ . From Eq. 15 we then find for the wind Lorentz factor  $\gamma_w < 5 \times 10^4$ . This has to be compared with the typical Lorentz factor of the particles at

$\epsilon_c$ , which is  $7.4 \times 10^5$ , and with the minimum Lorentz factor of injected particles that is  $< 500$ . The estimated value of  $\gamma_w$  translates into a lower limit on the pair multiplicity of  $\kappa \gtrsim 10^6$ .

Our model allows us to compute *a posteriori* the energy radiation losses. We do this in order to verify to what degree the adiabatic approximation for the evolution of the PWN radius is correct. For the Crab Nebula we find that about half of the total energy injected into the nebula in the form of pairs has been lost via synchrotron emission. However the dependence of the radius on the pulsar luminosity  $L(t)$  is in general weak (scales as  $L(t)^{1/5}$  for constant luminosity), so we expect at most modification of order 20% in the radial evolution, and maybe in the adiabatic losses. Such value is well within the simplifications and the approximations of the model. In order to properly take into account radiation losses, one needs to abandon any analytic solution for the dynamics, and solve the coupled system of equations for the dynamics and the emission simultaneously.

## 6.2 3C58

3C58 is another example of a young PWN, which shares many similarities with the Crab Nebula. It has a typical non-thermal spectrum extending from Radio to X-rays (Salter et al. 1989; Torii et al. 2000; Green & Scheuer 1992; Slane et al. 2004, 2008). It shows clear evidence of energy injection from the central pulsar PSR J0205+64 in the form of a *jet-torus* structure (Slane et al. 2002). Recent SPITZER measurements of the PWN IR luminosity have showed clear evidence for a possible injection break, like in the case of Crab (Slane et al. 2008). At a typical distance of 3.2 kpc (Chevalier 2005), its size is about  $5 \times 9$  pc, equivalent to a volume of  $\sim 140 \text{ pc}^3$  (corresponding to a spherical radius  $\sim 3.3$  pc). An association with the SN 1181 has been proposed (Stephenson & Green 2002). However recent measurements of the expansion of the filamentary structure surrounding the source (Bietenholz 2006; Rudie & Fesen 2007), interpreted through a simple model of the PWN-SNR sys-



**Table 2.** Values of the parameters corresponding to different models for 3C58

$\beta$	$\alpha$	$t$ (yr)	$M_{ej}$ ( $M_{\odot}$ )	$V_{SH}$ ( $\text{km s}^{-1}$ )
2	0	2000	5.4	270
2	1	2100	3.2	305
2	2	2250	1.2	355
2.33	0	2050	5.5	270
2.33	1	2180	3.3	307
2.33	2	2350	1.3	360

tem (van der Swaluw 2003; Chevalier 2005), have ruled out this possibility.

The pulsar present spin-down power is  $L \simeq 2.7 \times 10^{37}$  erg  $\text{s}^{-1}$ , with a characteristic dipole age  $t_c = 5390$  yr (Murray et al. 2002). Neither the true age nor the PSR braking index are known, and this prevents any reliable determination of the initial spin-down power. However it is possible to obtain some constraint from the information available on the expansion of the PWN and surrounding SNR. In particular, Bocchino et al. (2001) measured a mass in the filaments of  $\sim 0.1 M_{\odot}$ , and thermal emission corresponding to a typical shock velocity  $\sim 340$  km  $\text{s}^{-1}$ . Assuming that the filamentary structure corresponds to the swept-up shell of ejecta (in analogy with the case of the Crab Nebula) then we can use our model for the system evolution and obtain an estimate of both the system age and the PSR braking index depending on the density profile of the ejecta.

In Table 2, we present a set of models derived for different values of the unknown braking index (3 and 2.5), and for different density profiles of the ejecta. In all the different models the swept-up mass and the nebular volume are consistent with extant measures. The shock speed varies slightly, but is in all cases consistent with measurements, within the approximation of a spherical model. We again assume a canonical SN explosion energy of  $10^{51}$  erg. As in the case of Crab the lack of any clearly detected SNR shell prevents any reliable estimate of the ISM density and we simply assumed a fiducial value of  $0.1 \text{ cm}^{-3}$ .

By looking at Table 2, one immediately realizes that the inferred age is not very sensitive to either the braking index or the assumed ejecta structure. The reason for this is that in all cases the age is much less than the characteristic age, and the pulsar spin-down power in the past was not much larger than the present value. It is interesting to notice that in all models the shock speed tends to be higher for steeper ejecta, favoring the case  $r^{-2}$ . However this would result in a very small mass of the ejecta, inconsistent both with estimates based on the observed filamentary knots ( $\sim 8 M_{\odot}$ ) (Rudie & Fesen 2007), and with stellar evolutionary models.

It is our opinion that cases with a density profile which is either flat or  $r^{-1}$  are more likely, even if they are associated with a lower shock speed: this is because steeper ejecta lead to unreasonably small ejecta masses. In all cases the age estimated for the system rules out any association with SN 1181. However the filamentary structure, that we have interpreted as mostly due to swept-up ejecta, is rather complex and with various velocity components (Rudie & Fesen

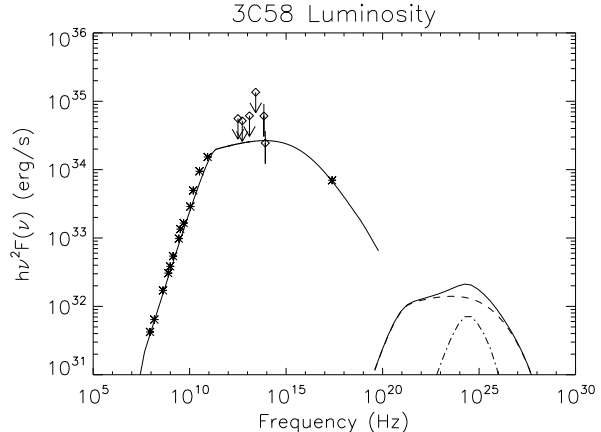


**Figure 2.** 3C58. Data points are: radio from Salter et al. (1989) Green & Scheuer (1992), X-ray from Slane et al. (2004), IR from Slane et al. (2008) (diamonds are IRAS and SPITZER points). Solid line is the total luminosity. Dashed line is the IC-CMB, dotted line is the IC-SYN.

2007), so that it cannot be ruled out that part of this filamentary network might be associated with the 1181 event.

The question that naturally arises is whether spectral fitting allows to discriminate between the models listed in Table 2. Unfortunately the answer is negative: fits to the observations lead to similar results in terms of the required injection parameters for all of these models. The reason is that all of them correspond to similar underlying ages, similar integrated spin-down power (*i.e.* total injected energy) and the same size (same adiabatic losses). The parameters reported in Table 1 correspond to the case of ejecta with  $\alpha = 1$  and braking index 3. Spectral fitting is shown in Fig. 2. Very similar values of the parameters are found also for a braking index of 2.5 ( $\beta = 2.33$ ).

If we compare the particle spectrum at injection with that of Crab, we find that the spectral index is now flatter at low energies and steeper at high energies. Again the required pair injection efficiency is very high  $\sim 80\%$  and the ratio  $\mu_e \sim 8.3 \times 10^{-5}$  is only a factor 2 lower than for Crab. The inferred magnetic field is  $43 \mu\text{G}$ , higher than other recent estimates (Slane et al. 2008). The ratio between the magnetic energy and the total energy is  $\sim 0.5$ , this is quite high and leads to a value for  $\eta_e + \eta_M > 1$  which apparently violates the total energetics. The discrepancy is however  $\sim 30\%$  and we consider it to be within the approximations of our model (particularly critical in this respect are the simplifications related to the assumption of spherical geometry) and the uncertainties of the data (especially the estimated distance, and hence volume). Models with  $\eta_e + \eta_M = 1$  always underpredict the radio emission, independently of the value chosen for  $\eta_M$ .

Within the present model, we consider our estimates of  $\eta_e$  and  $\eta_M$  rather solid: attempts at fitting the data assuming a lower magnetization and a higher particles' content result in underproduction of the radio emission, while larger magnetization leads to the break frequency moving below  $10^{11}$  Hz, in contrast with observations. One final remark we want to make about  $\eta_M$  is that the idea of a relatively high magnetization in this PWN is also supported by its sub-

stantial elongation, created by hoop stresses of the toroidal magnetic field (Begelman & Li 1992).

The existence of radio measurements down to 100 MHz allows us to derive also in this case a lower limit on the pair multiplicity: we find that  $\gamma_w < 3 \times 10^4$  to be compared with the typical Lorentz factor of the particles at  $\epsilon_c$ , which is  $1.2 \times 10^5$ , and with the minimum Lorentz factor of injected particles that is  $< 1600$ . This implies  $\kappa > 5 \times 10^5$ . All the latter values are very close to the corresponding estimates for Crab.

### 6.3 MSH 15-52

The system formed by the pulsar PSR B1509-58 and the SNR MSH 15-52 is striking for its relatively large size compared with its presumed age. Its distance is estimated to be  $5.2 \pm 1.4$  kpc (Gaensler et al. 1999). Assuming the central value as a fiducial distance (which we will do in the following), the SNR radius turns out to be  $\sim 83 \times 10^{18}$  cm. PSR B1509-58 is a young pulsar. Its current spin-down power is  $1.8 \times 10^{37}$  erg s $^{-1}$ , with a characteristic dipole age of 1550 yr (Kaspi et al. 1994; Livingstone et al. 2006). This is one of the very few pulsars for which the braking index is known:  $\beta = 2.087$ . Unfortunately, our ignorance of the true age of the system still prevents knowledge of the initial spin-down power,  $L_o$ : this can only be determined as a function of the assumed age,  $t$ . A maximum possible age of the system can be estimated from the braking index and the characteristic dipole age and the result is  $t < 1690$  yr. For such an age, the size of the SNR implies a high  $E_{SN}/M_{ej}$  ratio, typical of SN Ib/c (Gaensler et al. 1999; Tsvetkov 2002; Mazzali et al. 2000; Iwamoto et al. 2000; Mazzali et al. 2003; Tanaka et al. 2009). The size of the PWN is poorly constrained because of the high radio foreground from the SNR. Spectral modeling (Nakamori et al. 2008; Chevalier 2005; Du Plessis et al. 1995), however, suggests that the cooling frequency lies just below the *CHANDRA* band (see also the present discussion), which is also in agreement with the size of the nebula at TeV energies being comparable with the *CHANDRA* size. If cooling starts being important at frequencies no lower than the X-rays, then one can estimate the size of the PWN from *CHANDRA* images: the result is a PWN radius of  $\sim 17 \times 10^{18}$  cm, for the assumed distance.

Knowing the braking index, and assuming an age ( $t$ ) and an ejecta density profile ( $\alpha$ ), we can use our model to determine which values of  $E_{SN}$  and  $M_{ej}$  return the assumed radius for both the PWN and SNR. The only other parameter that enters this calculation is the local density of the ISM. We assume  $\rho_o = 0.001$  cm $^{-3}$ : a higher density would hint at even higher values of  $E_{SN}/M_{ej}$  and in any case does not allow to match both radii; a lower value marginally affects the results because the system turns out to be in the ejecta dominated phase anyway.

If one accepts the hypothesis that B1509-58 was born in a SN Ib/c explosion, then one can further constrain the model requiring that the mass of the ejecta is in the range  $4 - 10 M_\odot$ , and the kinetic energy released is in the range  $5 - 20 \times 10^{51}$  erg. In Tab. 3 we report the different age ranges. Flat ejecta tend to favor slightly younger systems. In spite of the relatively small differences between the ages reported in Tab. 3, spectral modeling can prove a useful tool to discriminate between different scenarios for this source. In the case of

**Table 3.** Different age ranges for models for B1509-58

$\beta$	$\alpha$	$t$ (yr) Size lim.	$t$ (yr) SED lim.	$\mu_e$
2.087	0	1350-1500	1470-1500	$1.2 \times 10^{-6}$
2.087	1	1570-1630	1570-1630	$2 - 4 \times 10^{-6}$

3C58 the inferred ages for all models were much smaller than the characteristic dipole age, so that the injection properties of the PSR were almost the same, and it was not possible to discriminate using the SED. On the contrary, for B1509, the inferred ages are close to the characteristic dipole age, and different models correspond to different spin-down histories, and different integrated injection energies. In such a situation the SED, and in particular the radio data, can be used to rule out some of the models allowed by the dynamics.

Observations cover the radio GHz band (Gaensler et al. 1999) (although the quality of the data in this band is not very high), X-rays from *CHANDRA* to *INTEGRAL* (Gaensler et al. 2002; DeLaney et al. 2006; Forot et al. 2006), *Fermi* in the MeV-GeV range (Abdo et al. 2010b), Cangaroo-II and *HESS* in the TeV (Nakamori et al. 2008; Aharonian et al. 2005). Only models with  $L_o > 10^{39}$  erg s $^{-1}$  can reproduce the radio, while lower values of  $L_o$  do not satisfy the energetic requirements. Tab. 3 shows the limits imposed on the model by SED fitting. Flat ejecta correspond to a very narrow range of possible ages and a value of  $\mu_e \sim 1.2 \times 10^{-6}$  smaller than what is found both for the Crab Nebula and 3C58. Vice versa, ejecta with  $\alpha = 1$  correspond to spin-down properties and multiplicity that are closer to what is found in Crab and 3C58. Compared with these two sources, we find a slightly harder high energy spectrum at injection  $\gamma_2 \sim 2.1 - 2.16$ . However, this is consistent with the hard spectrum observed in the MeV-GeV range by *Fermi* (Abdo et al. 2010b). Indeed the photon index derived from X-ray observations (Gaensler et al. 2002; DeLaney et al. 2006) of the inner region is  $\sim 1.4 - 1.6$ , and is much smaller than the previously used value  $\sim 2.7$  which seems inconsistent with both observations and energetics (Nakamori et al. 2008). Moreover the injection break is located between 5 and 50 GHz, at a significantly lower frequency than what was assumed in previous models (Nakamori et al. 2008).

Steeper ejecta give larger values of  $\mu_e$ , as reported in Tab. 3. All possible models require a high acceleration efficiency,  $\eta_e \sim 0.7$  and a strong magnetic field,  $\eta_M \sim 0.53$  implying  $B > 20 \mu\text{G}$ . Again, as in the case of 3C58, there is an energetic problem, but as in the previous case, this system is strongly magnetized, as also suggested by the presence of a strong X-ray jet (see Del Zanna et al. (2004) for a discussion of the dependence of the jet strength on the magnetization).

The lowest frequency radio point allows us to constrain the value of  $\nu_e$ , as it was done in Crab and 3C58. We find that even for  $\alpha = 1$ , the average wind Lorentz factor is  $\gamma_w < 10^4$ , quite small compared with other systems. This translates into a lower limit on multiplicity, that has to be greater than  $\sim 2 - 3 \times 10^5$ .

Fig. 3 shows the spectrum derived from the model presented in Tab. 1. From spectral fitting it is clear that the

Lorentz factor corresponding to  $\epsilon_c$  has to be smaller than  $5 \times 10^4$  ( $\mu_e$  has to be smaller than  $4 \times 10^{-6}$ ), otherwise it is not possible to reproduce the correct slope and intensity in the radio band (the injection break shifts below 1GHz). As a result  $\eta_M$  must be larger than 0.3, and the magnetic field cannot be smaller than  $15\mu\text{G}$ . Only by measuring the PWN emission in the range  $10^{10} - 10^{12}$  Hz, it would be possible to discriminate among various models and put better constraints on the multiplicity.

As it has already been noted (Aharonian et al. 2005) it is not possible to reproduce the observed gamma-ray emission in the TeV range, either with IC on the CMB or the average galactic background. The contribution from IC-SYN is negligible. Various models have been presented to account for such discrepancy.

One suggestion is that of a lower value of the magnetic field in the nebula, which would lead to infer a higher particle content, and consequently enhance the gamma over X-ray ratio (Aharonian et al. 2005). However, within this model this does not seem to be a viable solution: in order to increase the particle content up to the value required to fit the gamma-rays as IC on the standard galactic background we would have to violate the energetic fixed by the spin-down history by a factor  $\sim 5$ .

Another proposal is that of a possible contribution to the TeV flux of  $\pi^0$  decay, in the presence of relativistic hadrons (Nakamori et al. 2008). It was however immediately realized that this would require so much energy to be put in protons as to require millisecond magnetar conditions at birth for the pulsar, which seems unlikely judging from the present PSR-SNR properties. In addition, the swept-up ejecta do not provide a sufficient target density of thermal protons.

The third possibility is that the local photon background, in particular the IR, could be much higher than the average galactic value. Indeed the SNR itself could be the origin of this excess (Nakamori et al. 2008; Du Plessis et al. 1995). The fit presented in Fig. 3 assumes for the local IR background a black body with a temperature  $\sim 400\text{K}$  suppressed by a factor  $3 \times 10^{-7}$ , which corresponds to an energy density about 5-7 times higher than the average galactic background. It is interesting, in this regard, the suggestion by Helfand (2007) that the correlation between SNR detected by *HESS* and HII regions might be due to enhancements in the local photon background.

#### 6.4 Kes 75

The supernova remnant Kes 75 (G29.7-0.3) is a shell type remnant which hosts at its center a young PWN powered by pulsar PSR J1846-0258. This is a 324 ms pulsar, with a characteristic dipole age of 723 yr, a spin-down luminosity of  $8.3 \times 10^{36} \text{ erg s}^{-1}$ , and a measured value of the braking index  $\beta = 2.65$ , which provides an upper limit for the age of the system of  $\sim 880$  yr (Livingstone et al. 2006).

The estimated distance of the system suffers from large uncertainties. The first estimates pointed to a distance of 19-21 kpc (Becker & Helfand 1984). However it was immediately realized that such a large value implied very peculiar conditions for the Supernova explosion (Morton et al. 2007; Helfand et al. 2003) and the ISM, together with an extremely high synchrotron efficiency of the PWN. Recent

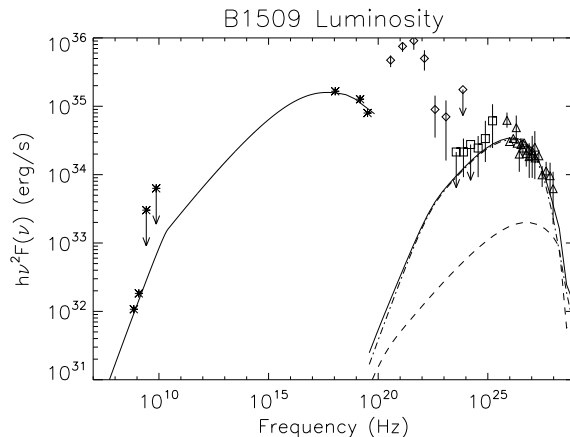


**Figure 3.** B1509-58; MSH 15-52. Data points are: radio from Gaensler et al. (1999), X-ray from Gaensler et al. (2002) DeLaney et al. (2006) Forot et al. (2006),  $\gamma$ -ray from Nakamori et al. (2008); Aharonian et al. (2005); Kuiper et al. (1999); Abdo et al. (2010b) (diamonds are *EGRET* points, squares are *Fermi* points, triangles are *COMPTEL/HESS* points). Solid line is the total luminosity. Dashed line is the IC-CMB, dash-dotted line is the IC on the enhanced local IR background at 400K.

studies have revised the distance to a much smaller value, in the range 5-7 kpc (Eisenhauer et al. 2005; Leahy & Tian 2008). We will assume a distance of 6 kpc in all our models.

Assuming a distance of 6 kpc, the radii of the PWN and of the SNR are, respectively,  $R = 1.8$  and  $R_{snr} = 9.24$  ly. The velocity of the forward SN shock is  $V_{SN} = 3700 \text{ km s}^{-1}$  (Helfand et al. 2006) as estimated via the Si X-ray line. This places an upper limit on the age of the system  $t < R_{SNR}/V_{SN} \sim 800$  yr. Various attempts have been made to measure the ejecta mass, and the SN energy; however the bulk of the SNR emission comes mainly from two regions of the SNR shell, and this tends to bias all estimates. In general, very high masses are inferred both for the swept-up ISM and for the SN ejecta (Becker & Helfand 1984; Morton et al. 2007; Leahy & Tian 2008), hard to reconcile with theoretical expectations for a SN Ib/c and standard evolutionary models. It must be stressed, however, that mass estimates are very sensitive to the assumed volume of the emission region, which is not well known.

Proceeding as for previous cases, we will first attempt to constrain the possible SNR-PWN parameters through models for the dynamical evolution of the system. Given an assumed age  $t$  and an ejecta profile  $\alpha$  there is only one set of values of  $E_{SN}$ ,  $M_{ej}$  and  $\rho_o$  that gives the correct size of both the PWN and the SNR and the correct forward shock speed. Further constraints on the parameter space come from the properties of SN Ib/c which limit  $M_{ej}$  in the range  $5M_{\odot} \lesssim M_{ej} \lesssim 16M_{\odot}$ . Cases with  $\alpha \geq 1$  are acceptable only for a system older than 700 yr, and are in general unlikely because they require a very low SN energy,  $E_{SN} \lesssim 0.3 \times 10^{51} \text{ erg}$ . Cases with flat ejecta are admissible for a larger range in age from 450 yr to 650 yr. The typical SN energy does not seem to depend on the age and is  $E_{SN} \sim 2 \times 10^{51} \text{ erg}$ ; younger systems require lower values of  $M_{ej}$ , and larger values of  $\rho_o$ , as shown in Tab. 4. Cases with marginally steep ejecta,  $\alpha = 0.5$  suggest a larger age,

**Table 4.** Different age ranges for models for Kes75

$\alpha$	$t$ (yr)	$M_{ej}$ ( $M_\odot$ )	$\rho_o$ ( $\text{cm}^{-3}$ )
0	450	4.8	4
0	550	8.0	3
0	650	16.4	2
0.5	600	4.6	0.8
0.5	700	10.7	0.5

a less energetic explosion,  $E_{SN} \sim 0.6 \times 10^{51}$  erg, and lower ISM density.

The question arises again of whether it is possible to discriminate among the different parameter sets for the dynamics based on the SED. Unfortunately this is not the case: as it was already realized earlier (Chevalier 2004), Kes 75 is a particle dominated system by large (more than 90% of the pulsar spin-down power seems to be converted into accelerated particles, see below), so the differences in particle content due to the different energetics of the various models can be easily compensated by small changes in the magnetization to give the same synchrotron emission.

However, fitting the model to the multi-band emission spectrum is non-trivial. The radio emission spectrum implies a low energy particle spectral index at injection  $\gamma_1 = 1.7$  (Becker & Helfand 1984; Salter et al. 1989; Bock & Gaensler 2005). The average photon index in the *CHANDRA* band is 1.9 while deep X-ray images have shown that the photon index in the vicinity of the pulsar is  $\sim 1.8$  (Blanton & Helfand 1996; Collins et al. 2002; Helfand et al. 2003; Ng et al. 2008).

Evidence for a possible spectral break below 100 GHz was presented by Bock & Gaensler (2005), but these data seem to be inconsistent with previous measurements (Salter et al. 1989) and a single power-law cannot be ruled out.

Indeed in our model an injection break below 100GHz would require a very hard high energy injection, inconsistent with spectral information at X-ray frequencies. IR data do not provide good constraints (Morton et al. 2007). *INTEGRAL* data above 15 keV show a particularly hard spectrum, not fully consistent with an expected cooling break in the *CHANDRA* band (Terrier et al. 2004), but the pulsar might contribute to the flux above 40 keV and be responsible for the excess emission at high energies.

If the X-ray emission in the *CHANDRA* band corresponds to freshly injected high energy particles, one must infer  $\gamma_2 > 2.6$ . However we found that it is not possible to fit the overall SED when adopting such a soft high energy injection. The reason is simple: given that the average spectral index is close to the one measured at the injection, the synchrotron break frequency must be above the *CHANDRA* band, but this implies a magnetic field  $B \lesssim 10\mu\text{G}$ . Even assuming  $\eta_e = 1$ , with this small field all the models underproduce the radio emission by at least a factor 5. We find that it is possible to fit the synchrotron spectrum, including the average slope in the X-rays, only if  $2.2 \leq \gamma_2 \leq 2.4$ .

As to the other parameters, we notice the following: the value of  $\eta_M$  depends on age, with younger systems ( $t \sim 450$  yr) requiring a field  $B \sim 30\mu\text{G}$ , and older ones ( $t \sim 650$

yr) requiring  $B \sim 20\mu\text{G}$ , but it does not depend on  $\gamma_2$ ; the value of  $\mu_e$  depends on  $\gamma_2$ , ranging from 4000 for  $\gamma_2 = 2.4$  to  $4 \times 10^4$  for  $\gamma_2 = 2.2$ , but it is independent of age. All the models require a very high injection efficiency  $\eta_e \sim 1$ , to reproduce the *INTEGRAL* points. In Fig. 4, we show the spectrum derived according to the model in Tab. 1.

The Lorentz factor corresponding to  $\epsilon_c$  ranges between  $2 \times 10^5$  and  $1.5 \times 10^6$ , very close to the values derived in Crab. The one corresponding to the model of Fig. 4 is  $7 \times 10^5$ . The minimum Lorentz factor is lower than  $\sim 5 \times 10^4$ , and the average Lorentz factor is  $\sim 7 \times 10^4$ , with an associated multiplicity that has to be greater than  $10^5$ .

Kes 75 has been detected in gamma rays by *HESS* (Terrier et al. 2008; Djannati-Atai et al. 2008). The particles responsible for TeV gamma-ray emission, in a purely leptonic model, are the ones emitting synchrotron radiation in the *CHANDRA* band. However the photon index in the TeV range is found to be  $\sim 2.3$ , far steeper than the average X-ray photon index of 1.9. Inverse Compton scattering on local synchrotron radiation gives a negligible contribution of TeV gamma-rays. Despite this being a young system, PSR J1846-0258 has a low spin-down luminosity, which results in a particle content about 2 orders of magnitude lower than in Crab and a correspondingly lower energy density of the synchrotron photon field. Inverse Compton scattering on CMB photons is about 50 times stronger. However, even this contribution is about a factor of 10 below the observed flux. In addition, scattering on the CMB is expected to occur in the Thompson regime and cannot account for the steepening of the spectral index in gamma-rays. A suggestion that has been made is that this steeper spectrum hints at a much warmer radiation background, for which IC should take place in the Klein-Nishina regime. This requirement places the average black-body temperature of the seed background photons in the range 1000-2000 K.

With a black-body spectrum at 1000 K, suppressed by a factor  $5 \times 10^{-9}$ , it is possible to reproduce the correct gamma-ray luminosity. This contribution corresponds to a local enhancement of the infrared background which is only a factor of a few above the galactic average. Interestingly, as in the case of B1509, also Kes 75 is surrounded by a bright SNR shell, that might be responsible for the enhancement.

The question arises if the TeV gamma-rays can be explained by a hadronic component, and in particular by  $\pi^0$  decay. Given the very low magnetization, inferred from the synchrotron spectrum, it can be shown that only weak constraints can be put on  $\eta_p$ ; in particular one can obtain a good fit of the radio and *CHANDRA* X-ray data, using  $\eta_e \sim 0.5$  (which however underpredicts *INTEGRAL* data) and a slightly higher nebular field, without violating the energetics. However even by assuming half of the spin-down energy goes into protons, in order to have a significant contribution to the emission in the 10TeV range, at least  $10M_\odot$  of target thermal protons are needed. This is far in excess of the swept-up ejecta mass  $\sim 0.1M_\odot$ , even if consistent with the total ejecta mass (in this case one needs to assume that protons escape from the PWN and interact with the SNR). The main problem in this case is to properly reproduce the observed TeV spectrum: our model predicts a peak at  $10^{28}$  Hz, instead of  $10^{25}$  Hz as is observed, which is due to our choice of injection energy for the protons, which is tied to  $\gamma_w$ . *Fermi* observations should be able to distinguish between a

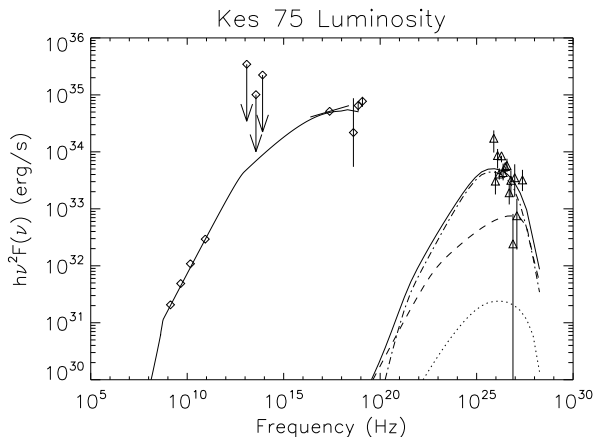


**Figure 4.** Kes75; SNR G 29.7-0.3. Data points are: radio and IR from Becker & Helfand (1984); Salter et al. (1989); Bock & Gaensler (2005), X-ray from Collins et al. (2002); Terrier et al. (2004),  $\gamma$ -ray from Terrier et al. (2008); Djannati-Ataï et al. (2008). Solid line is the total luminosity. Dashed line is the IC-CMB, dash-dotted line is the IC on the enhanced local IR background at 1000K. Dotted line is the IC-SYN.

leptonic and a hadronic model, by constraining the emission below 1TeV. To properly investigate whether  $\pi^0$  decay is a viable possibility to explain the gamma-ray data, one would need a model for the diffusion of protons outside the nebula, which at the moment we do not have. The simplest possible estimate of the diffusion time of protons outside the nebula, and in the ejecta, gives values that are about an order of magnitude larger than the age of the nebula.

## 6.5 Old Objects

In this section we discuss two relatively old objects. The code has been developed for the investigation of systems also beyond the free expansion phase. However the late dynamics, especially if the pulsar kick velocity is important, can be quite complex. In addition old systems are usually very poorly constrained from the observational point of view. The age is generally known only as an order of magnitude estimate, and quite often either the central pulsar is not observed (as in the case of G327.1 and IC443), or the SNR is not observed.

The following discussion highlights the difficulties that one has to face when trying to model sources for which both the quantity and the quality of the data are really poor.

### 6.5.1 W44

The SNR W44 is known to contain an old PWN, associated with pulsar PSR B1843+01. This is a 267 ms pulsar, with a characteristic dipole age of 20,380 yr, and a spin-down luminosity of  $4.3 \times 10^{35}$  erg s $^{-1}$  (Wolszczan et al 1991). The value of the braking index is not known, while the distance of the pulsar is estimated to be 3.1 kpc (Wolszczan et al 1991) for a typical electron density  $0.03$  cm $^{-3}$ .

The SNR W44 (3C 392) has an elongated shape with axes  $25' \times 11'$ . Its distance is estimated from HI absorp-

tion to be 2.6 kpc, corresponding to a typical SNR radius of 11–13 pc (Cox et al. 1999). The small discrepancy between the estimated distance to the PSR and to the SNR is within the uncertainties, and the association is considered a secure one. This is a post-reverberation system, for which pressure balance between the PWN and the SNR is important. The central pressure is estimated from X-ray observations to be  $\sim 1.4 \times 10^9$  dyne cm $^{-2}$  (Cox et al. 1999). Modeling the SNR (Cox et al. 1999; Shelton et al. 1999) leads to the following estimates for the relevant dynamical parameters:  $E_{SN} = 10^{51}$  erg,  $M_{ej} = 5M_{\odot}$ ,  $\rho_o \sim 6$  cm $^{-3}$ ; for the expansion velocity of the SNR, HI emission gives  $v_{fs} \sim 150$  km s $^{-1}$  (Koo & Heiles 1995). A couple of remarks are here in order: first, all existing models assume the spin-down time of the pulsar as the age of the nebula; second, the quoted value of  $v_{fs}$  is inferred from a HI emitting ring structure which does not trace exactly the SNR, and estimates of the remnant speed can be as high as 330 km s $^{-1}$  (Koo & Heiles 1995).

The PWN is observed in radio (Frail et al. 1996; Giacani et al. 1997) with a typical luminosity of 200 mJy. It has a distinctive cometary shape with the pulsar located at the tip of a protruding finger of emission. The nebula is thought to be a transition object from the spherical shape of young systems to later bow-shock like morphologies (van der Swaluw et al. 2004). Within this picture it is assumed that the PWN has already been crushed by the reverse shock, and that the pulsar has been displaced by its proper motion with respect to the core of the radio emission. X-rays have been detected both with *CHANDRA* and *XMM-Newton* from the head of the cometary nebula in the vicinity of the pulsar (Petre et al. 2002; Harrus et al. 2006), and the flux is measured to be  $\sim 2.7 \times 10^{-13}$  erg cm $^{-2}$  s $^{-1}$  in the 2-10 keV band (Harrus et al. 2006; Petre et al. 2002). The radio emission is about twice as extended as the X-rays, suggesting effective cooling in the nebula, for which, however, there is no indication from the spatial behavior of the spectral index: this is found to be  $\sim 2.2 \pm 0.3$  with no appreciable variations with the distance from the pulsar (Harrus et al. 2006). No IR or  $\gamma$ -ray emission is detected. At low radio frequencies the PWN is too weak to be detected against the SNR.

The PWN is quite weak compared to the pulsar spin-down energy, and appears also to be quite small in size, even if a correct determination of the volume is problematic, given the shape. At the distance of the SNR, a typical value for the volume is  $\sim 0.5$  pc $^3$ , corresponding to a radius  $\sim 1.5$  ly. It is interesting to notice that models of the PWN have often assumed a much smaller age  $< 5000$  yr (Petre et al. 2002), in order to fit the observed spectrum, which clearly contradicts what has been used to model the SNR. However such models are usually developed assuming that the spectrum is Crab-like (in terms of the ratio between the radio and X-ray emission, and in terms of the location of the cooling break), but as we have shown through our modeling of young systems things can be different in different objects.

The major problem in modeling this system, as was already recognized by Petre et al. (2002), is the relatively low radio luminosity compared to the energy content of the nebula, and to the integrated pulsar spin-down power. This suggests that probably the age of the system is much lower. As a general rule, a younger age and a braking index less

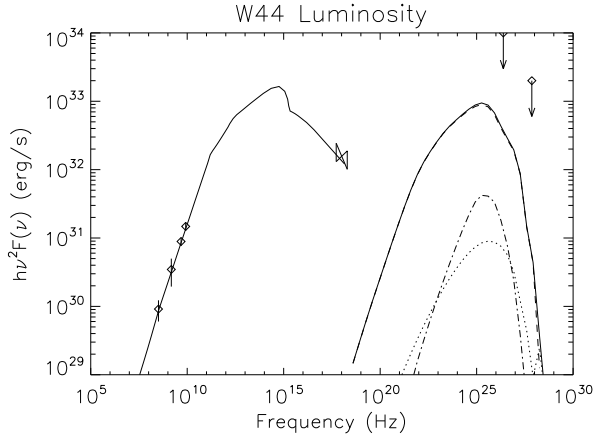


**Figure 5.** W44. Data points are: radio from Frail et al. (1996); Giacani et al. (1997), X-ray from Petre et al. (2002); Harrus et al. (2006), upper limits on  $\gamma$ -ray from Aharonian et al. (2002); Abdo et al. (2009b). Solid line is the total luminosity. Dashed line is the IC-CMB, dash-dotted line is the IC on the local IR background (same as for Crab nebula). Dotted line is the IC-SYN.

than 3 correspond to less injected energy. In particular, we find that a braking index close to 2 and an age of about 10,000 – 15,000 yr are required to reproduce the observed radio emission. We also require that the average magnetic field in the nebula must be well below equipartition. Indeed we find that, in order to avoid overproducing the radio emission,  $\eta_M$  has to be  $< 0.002$ , corresponding to a nebular field below 10  $\mu$ G, even if in principle this refers to the average magnetic field, while the value in the head can be higher.

This small value gains some support from the lack of spectral steepening with distance, which suggests that cooling is not important. Indeed the difference in size between the radio and X-ray nebula could be explained by the presence of a much stronger magnetic field in the head of the nebula than in the body, resulting in the suppression of X-ray emission in the latter. In Table 5 we list the values of the parameters used to produce the curve in Fig. 5. Values of the SNR parameters are not dissimilar from what has been used in the literature (Cox et al. 1999; Shelton et al. 1999). The value we find for the central pressure is  $\sim 1.6 \times 10^9$ , in agreement with X-ray observations, but the expansion speed is found to be higher,  $v_{fs} \sim 300 \text{ km s}^{-1}$ , as a consequence of the younger assumed age.

It is evident that the quantity and quality of existing data do not allow us to constrain the PWN model as much as it is possible for younger systems. Moreover, the shape is far from spherical, and geometrical effects connected with the existence of a bow shock cannot be modeled correctly within our approach. However, by repeating the same analysis we did in the previous section, we find that the parameter  $\mu_e$  in the model is  $8 \times 10^{-3}$ , which corresponds to a Lorentz factor at  $\epsilon_c$  equal to  $2 \times 10^5$ , while the average wind Lorentz factor is found to be  $\gamma_w \lesssim 10^4$ , corresponding to a multiplicity  $\kappa \gtrsim 10^5$ .

One thing to notice is that the spectrum barely extends to X-ray frequencies. As pointed out above, this is due to the low value of the magnetization we adopt. If the magnetization in the head is higher, as could be expected due to

compression in the bow shock, this might enhance the X-ray emission.

Another striking feature is the bump at around  $10^{15}$  Hz: this is a typical feature of post-reverberation systems. During the reverberation phase, there is a typical energy at which synchrotron losses are balanced by adiabatic compression gains. Particles tend to accumulate at this energy, and this causes a bump in the spectrum, which survives at later times. One final point of interest is the fact that for this system (and for relatively old systems in general) IC scattering on the CMB gives a TeV flux that is comparable with that in the X-rays.

### 6.5.2 K2/3 Kookaburra

The “Kookaburra” is a complex of compact and extended radio/X-ray and  $\gamma$ -ray sources, that spans about one square degree along the galactic plane. A large circular thermal shell with a broad wing in the North-East and a narrower one in the South-West is revealed from radio images. Diffuse X-ray emission and point like sources have been detected by *ASCA* (Roberts et al. 1999, 2001), *XMM-Newton* and *CHANDRA* (Ng et al. 2005). We are here interested in the North-East wing where at radio and X-ray frequencies a nebula is found, hosting a young and energetic pulsar, PSR J1420-6048. The pulsar location is also coincident with TeV  $\gamma$ -ray emission detected by *HESS* (Aharonian et al. 2006).

PSR J1420-6048 is a 68.2 ms pulsar, with a characteristic dipole age of 13,050 yr and a spin-down luminosity of  $10^{37} \text{ erg s}^{-1}$  (D’Amico et al. 2001). The braking index is not known: as for the case of W44, this implies that the true age could differ substantially from the characteristic dipole age. The distance of the pulsar is estimated to be  $5.5 \pm 0.8 \text{ kpc}$  (Aharonian et al. 2006).

Identifying the PWN associated with PSR J1420-6048 is, however, rather problematic. The wing-like structure hosting the pulsar is usually referred to as K2. In coincidence with the PSR an enhancement of radio emission, usually referred to as K3, is also observed. K2 has an extent of  $\sim 15' \times 10'$ , a total flux at 20 cm of  $\sim 1 \text{ Jy}$ , and a spectral index  $0.2 \pm 0.2$ , while K3 has an extent of about  $3'$ , a total excess flux at 20 cm of  $\sim 20 \text{ mJy}$ , and a spectral index  $0.4 \pm 0.5$  (Roberts et al. 1999). No IR detection has been reported.

X-rays have been detected by *ASCA* in the 2-10 keV band, with an extent of about  $7'$ , an integrated flux of  $4.8 \times 10^{-12} \text{ erg cm}^{-2} \text{ s}^{-1}$ , and a spectral index 1.4 (Roberts et al. 2001). A much more compact ( $0.5'$ ) but extended source has been detected by *CHANDRA* around the pulsar, with a total flux, extrapolated to the 2-10 keV band, of  $1.3 \pm 0.14 \times 10^{-12} \text{ erg cm}^{-2} \text{ s}^{-1}$ , and with a spectral index  $2.3 \pm 0.9$  (Ng et al. 2005).

Gamma-rays were first detected by *EGRET* (Thompson et al. 1996), and more recently by *HESS* (Aharonian et al. 2006). The total *HESS* luminosity in the 0.4-20 TeV band is  $5.1 \times 10^{34} \text{ erg s}^{-1}$ , for the assumed distance, and the spectral index is found to be  $\sim 2.2$ . The  $2\sigma$  angular extension of the gamma-ray emission ( $\sim 7'$ ) implies a nebular size  $\sim 11 \text{ pc}$ .

One immediately realizes that from a dynamical point of view these data are somewhat confusing. In particular we think that the standard interpretation, according to which

**Table 5.** Model parameters for W44 and K2/3 corresponding to the curves in figures 5 and 6. Units are the same as in Tab. 1.

Obj.	$t$	$E_{SN}$	$M_{ej}$	$\rho_o$	$\alpha$	$L_o$	$\tau$	$\beta$	$\gamma_1$	$\gamma_2$	$\eta_e$
W44	15000	1	5	3	0	0.018	22000	2.82	1.3	2.55	0.85
K2/3	8000	1	8	0.2	0	0.34	13750	2.66	1.2	2.82	0.95

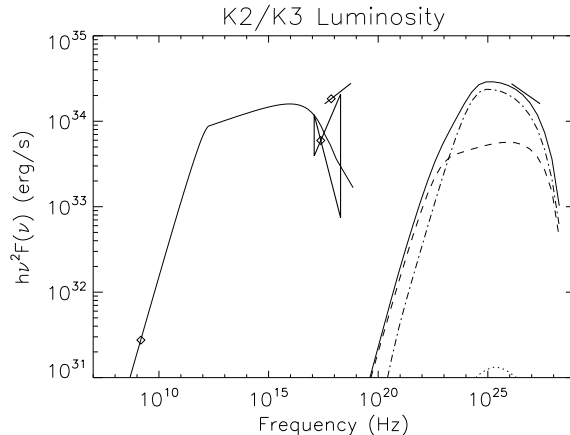
the small K3 region is the PWN, while the K2 region is the SNR Roberts et al. (2001), seems unlikely. Indeed, within the framework of our model, this assumption leads to unphysical values for the supernova energy and ejecta mass and to overpredict the radio emission.

The larger extent of the *ASCA* source, compared to the *CHANDRA* one, goes against the expectation that the nebular size should shrink at higher frequencies because of synchrotron cooling. The difference in *ASCA* and *CHANDRA* spectral index might be due to uncertainties on the assumed value of  $N_H$ . The spectral index of the TeV emission (interpreted as IC-CMB) is consistent with the steeper *CHANDRA* spectrum, but not with the flat *ASCA* one.

Even the radio data are not conclusive: if one assumes that the PWN also contributes to the K2 emission, rather than just to K3, the radio emission changes by about 2 orders of magnitude. The uncertainties in the age, size and interpretation of the observed fluxes, in addition to the lack of a well defined SNR, seriously hamper the modeling of the system. Indeed, as for W44, we will present here just a simple model fit to the data, without going into any detailed investigation of the parameter space.

Again, as in the previous case, the major difficulty in accounting for what is observed relates to the low efficiency both in X-rays and radio, together with the ratio  $L_\gamma/L_X > 1$ , which is suggestive of a large nebular content of low-energy particles. As in the case of W44 this implies that a decent fit to the data can only be achieved if one assumes a relatively young system, with a steep high energy spectrum (similar to 3C58) and a weak magnetization (comparable with that in Kes75). Fig. 6 shows the result of the model corresponding to the parameters in Tab. 5. The nebular radius is found to be  $\sim 5$  pc in agreement with the *HESS* size. The magnetic field is inferred to be  $\sim 5\mu\text{G}$ . It is clear that it is not possible to reproduce simultaneously the *CHANDRA* and *ASCA* data. To get the steeper *CHANDRA* spectrum one needs to assume a cooling break around  $10^{16}$  Hz. This is also necessary in order to reproduce the correct TeV spectrum. As already suggested by Aharonian et al. (2006), in the TeV range the IC-CMB dominates over the IC on the standard galactic background. Indeed our model under-predicts the TeV emission by a factor 4-5. The local photon background must be higher if the observed TeV flux has to be explained as IC emission: the TeV flux shown in Fig. 6 was obtained by assuming an IR background in the form of Black-Body at 200K, with a photon density about a factor 4-5 higher than the standard galactic background. Given the complexity of the Kookaburra region, one cannot exclude such possibility.

The parameter  $\mu_e$  in the model is found to be  $5 \times 10^{-5}$ , which corresponds to a Lorentz factor at  $\epsilon_e$  equal to  $2 \times 10^5$ , while the the average wind Lorentz factor is  $\gamma_w \lesssim 10^4$ , corresponding to a multiplicity  $\kappa \gtrsim 10^5$ .

**Figure 6.** K3/2 Kookaburra. Data points are: radio from Roberts et al. (1999), X-ray from Roberts et al. (2001),  $\gamma$ -ray from Ng et al. (2005); Aharonian et al. (2006). Solid line is the total luminosity. Dashed line is the IC-CMB, dash-dotted line is the IC on the local IR background (assumed as a black body at 200K). Dotted line is the IC-SYN.

## 7 DISCUSSION & IMPLICATIONS

Let us briefly review here our findings, and what general conclusions can be drawn from the results of our attempt at modeling different objects, both young and old.

### 7.1 Summary of the results

First of all, it is remarkable that our one-zone model, despite its simplifications, has proven able to account for the observed Spectral Energy Distributions in all cases. This is already an interesting result, since the assumption of efficient mixing that is at its base is likely a poor approximation at high energies (in the X-ray band), where the flow pattern and the magnetic field structure in the inner nebula are expected to play a dominant role.

The agreement between the model fit and the data is extremely good in the case of Crab, where the unknown parameters are reduced to a minimum (essentially the SNR properties). Our model seems to work rather well for young systems in general, but the quality of the data and the limited spectral coverage lead to larger uncertainties. In the case of strongly magnetized sources, like 3C58 and the nebula associated to PSR B1509, we find that in order to reproduce the data our model requires an energy input in the PWN which exceeds the pulsar release by 20-30%, judging from the current spin-down power. This conclusion does not seem to be affected by uncertainties in the distance to the sources: moving them closer to (further from) us would lower (increase) the estimated brightness, but at the same time it

**Table 6.** Summary of the inferred lower limits on multiplicity.

Crab	3C58	MSH 15-52	Kes75	W44	K2/K3
$10^6$	$5 \times 10^5$	$3 \times 10^5$	$10^5$	$10^5$	$10^5$

would make them smaller and younger (larger and older), leaving the discrepancy between the radiated and accumulated energy almost unaltered. We think it likely that this discrepancy is due to the simplifying assumptions of the one-zone model, which become progressively more important at large magnetizations. In particular, as also shown by recent multidimensional simulations (Volpi et al. 2008), the radio and X-ray emitting particles might sample different magnetic fields. At the same time it is worth keeping in mind that the estimate of the PSR spin-down power is based on the assumed canonical moment of inertia for neutron stars:  $I = 10^{45} \text{ g cm}^2$ . A 20% discrepancy in two systems is compatible with present uncertainties.

As one can easily see from Tab. 1, given the already high value of the quantity  $\eta_e + \eta_M$ , there is little energy ( $\sim 20\%$  at most) left to be carried by any other higher energy component (ions or leptons in the return current). The idea that a particle population with a larger Larmor radius could be carrying most of the wind energy was made attractive by the following three main reasons: these particles could help solve the problem of particle acceleration at the pulsar wind termination shock; they could explain the wisps variability in the Crab Nebula; finally, in the case of ions, they could solve the discrepancy between the predictions of 1-d MHD models and the gamma-ray flux observed from Crab.

As far as particle acceleration is concerned, at a relativistic pair shock, efficient acceleration is shown to be possible only if the shock magnetization is extremely low (Spitkovsky 2008). The 2-D MHD models of PWNe (Del Zanna et al. 2006; Camus et al. 2009), use a simple model of field reversal across the equator where a current sheet occurs, such that the appropriate conditions for acceleration are thought to be realized only in a small sector of the pulsar wind termination shock, with no more than a few percent of the total wind energy flux flowing through it.

On the other hand, the presence of an energetically significant ion component in the pulsar wind is found to lead to efficient acceleration of the pairs (Hoshino et al. 1992; Amato & Arons 2006). This effect is the consequence of the large Larmor radius of the ions, whose gyration introduces long wavelength turbulence through cyclotron instability. The same result could come from the presence of high energy leptons, accelerated as a consequence of runaway dynamics in the equatorial current layer (Arons, in preparation).

As to the wisp variability, Spitkovsky & Arons (2004) showed that this could be explained as the result of compression waves associated with the high energy current carriers' (ions, in their case) gyration in the shock region: in order to reproduce the observed brightness contrast, again one would need the current carriers (the "beam") to be energetically significant:  $\gamma_{\text{beam}} m_{\text{beam}} / \gamma_w m_{\pm} > 2\kappa_{\pm}$ . An alternate explanation of the wisp variability, which does without the kinetic effects of the high energy particles beam, has been recently shown by Camus et al. (2009), who have proved that it can

be recovered also within the framework of pure MHD, due to global instabilities of the termination shock.

One final consideration concerns the possible detection of signatures of high energy protons. Modeling of the TeV emission from the Crab Nebula, based on the 1D Kennel & Coroniti flow (Atoyan & Aharonian 1996) was shown to underpredict the observed flux by a factor  $\sim 5$ , leading to suggest a possible contribution from the decay of neutral pions produced in nuclear collisions of relativistic protons. More recently, the presence of relativistic protons as the source of high-energy gamma-ray emission was suggested also in the Vela PWN (Horns et al. 2006). In the case of Vela, however, a later determination of the density of the thermal protons (that would serve as a target for nuclear collisions) resulted in too low a value and led to strongly question the initial claim (LaMassa et al. 2008). At the same time, Volpi et al. (2008) showed that using a multidimensional model for the flow structure in Crab, the estimated IC-TeV emission is easily overproduced, for the same parameters that allow one to better fit the lower energy synchrotron emission. This suggests that the results are indeed strongly model-dependent and that the discrepancies are likely due to problems with the adopted MHD model.

This is also the conclusion we reach in this work. We can reproduce the TeV emission from Crab, and find results in agreement with *Fermi* observations without any need for a proton contribution. In the case of both B1509 and 3C58, our pair+magnetic field energetic is already exceeding by 20% the estimated PSR energy input, and fitting the gamma-rays through  $\pi^0$  decay requires that protons alone carry far more energy than the nebula is currently estimated to store. Finally, in the case of Kes75, in order to ascribe the excess TeV emission to protons, one needs to assume that protons can effectively diffuse out of the nebula and experience the whole ejecta mass as a target.

Our model seems to constrain with good accuracy the value of  $\epsilon_c$ . It is not possible to vary the value of  $\epsilon_c$  by more than a factor of a few still satisfying the overall energetics and reproducing the radio and X-ray data. At the same time, our model allows us to derive, for each object, an upper limit on the wind Lorentz factor and a lower limit on the pair multiplicity. The limits we put on  $\gamma_w$  and  $\kappa$  are strictly valid only if the wind has a unique Lorentz factor and the energy scales  $\epsilon_m$  and  $\epsilon_c$  respect the assumed scaling with time, proportional to the pulsar voltage. It is not easy to predict how a possible latitude dependence of the wind Lorentz factor, such as that included in axisymmetric models of PWNe (e.g. Del Zanna et al. (2004)), or a different dependence on time of the energy scales would affect our conclusions.



## 7.2 Interpretation of spectral breaks

Our study has reinforced a long standing puzzle: the electron (and positron) accelerator at work in PWNe knows how to create a spectrum convex in energy space, best represented by a broken power law. As was advanced by Kennel & Coroniti (1984b), the spectral steepening observed between optical/soft X-ray energies and the harder ( $\varepsilon > 10$  keV) spectrum is well understood as the effect of synchrotron energy losses, with the pre-cooled spectrum a power law  $N(E) \propto E^{-\gamma_2}$ ,  $2.1 < \gamma_2 < 2.8$  from Table 1. The steepening between mid-infrared and optical, when observed, requires energy space structure in the accelerator (an “intrinsic break”). The high energy spectrum can be attributed to diffusive acceleration at the termination shock, at least qualitatively - Fermi acceleration in relativistic very low sigma shocks in the test particle limit yields a spectrum  $N(E) \propto E^{-2.2}$  (Keshet & Waxman 2005). The radio spectrum requires a much harder distribution of the lower energy particles,  $N(E) \propto E^{-\gamma_1}$ ,  $1.2 < \gamma_1 < 1.7$ .

The standard model Kennel & Coroniti (1984a,b), developed to account for the radiation from Crab at near infrared and shorter wavelengths, assigns the conversion of the pulsar wind energy in the particle spectra that emit the observed synchrotron radiation to diffusive Fermi acceleration at the wind termination shock. Diffusive shock acceleration always shows particle spectra with a Maxwellian at low energy, plus a power law supra-thermal tail at high energy, with the temperature of the Maxwellian set by the shock jump conditions (except when the acceleration of the tail is very efficient). These properties are well exhibited by Particle-in-Cell simulations of relativistic shocks in *unmagnetized*  $e^\pm$  plasmas (or, if magnetized, in upstream quasi-parallel flow geometry (Spitkovsky 2008; Sironi & Spitkovsky 2009)). Our models identify the transition between the soft, high energy spectrum and the hard, low energy spectrum as being at the energy  $\epsilon_c$ , typically  $10^5 - 10^6 m_\pm c^2$  (see Table 1). In the (Kennel & Coroniti 1984b) model, this energy was identified as the lower cut-off of the shock accelerated power law, and that energy was identified as the “temperature”  $\approx \gamma_w m_\pm c^2$  of the flow downstream of the termination shock, thus giving rise to the belief that pulsar winds have upstream flow Lorentz factor  $\gamma_w \sim 10^6$ .

The Kennel and Coroniti model and its descendants deliberately neglected the radio emission from the Crab Nebula (and, by extension, other PWNe.) The large (by number) population of particles with  $E < \epsilon_c$  suggests  $\gamma_w$  to be much smaller, if the radio and mid- to far-IR emitting particles come from the pulsar. That the pulsars are the most likely source of the low energy particles in each of the nebulae gains support from the existence of the radio “wisp” features in the Crab (Bietenholz 2004) closely associated with the similar time variable structures seen in optical and X-ray imaging, as well as similar structure seen in 3C58 (Bietenholz 2006) - those structures are clearly coincident with the termination shock. Then, in the regions of the flow populated by the large particle flux feeding the low energy population,  $\gamma_w \sim 10^4$  or smaller.

The low energy particle spectrum definitely is not a single temperature relativistic Maxwellian, with  $T \sim \epsilon_c$ . Since the termination shock is not spherical, becom-

ing more oblique in higher rotational latitude regions (Komissarov & Lyubarsky 2004; Del Zanna et al. 2004), the post-shock temperature declines with increasing latitude, suggesting the low energy particles enter in the polar regions of the outflow. However, replicating the observed spectrum as the envelope of a sequence of Maxwellians requires a factor of  $\sim 100$  variation in temperature, which requires most of the mass flux being nearest the rotation poles. There is no sign of pole to equator asymmetry in the radio emission near the pulsars, except for the radio wisp features in the Crab, which are components of the immediate post-shock flow, as judged from the optical and harder photon emission. However we cannot rule out that mixing and effects related to integration along the line of sight might prevent the detection of the implied variations.

However, let us assume in the following, that also the low-energy particle spectrum results from some acceleration process, rather than from the convolution of different thermal distributions, and let us speculate on the nature of such a process.

Turbulence and associated Fermi II acceleration in and around the termination shock is one appealing possibility. The “wisp” motion, observed from the radio through X-rays (see Hester (2008) for a comprehensive review) has recently been interpreted as the result of the strongly variable termination shock structure found in high resolution MHD simulations of the Crab Nebula (Camus et al. 2009). The shock instability implied is a termination shock variant of the Standing Accretion Shock Instability, with outer scale variable velocity  $\delta v \sim v \sim 0.6c$  and length scale  $\delta r \sim r \sim 0.5 - 1$  light years. The magnetized motions observed in the simulations (which do well in replicating the time variable spatial structure observed in the nebular “wisps”) can act as an accelerator through the Fermi II process (Kardashev 1962; Stawarz & Petrosian 2008), creating electron and positron spectra  $N(E) = N_0(E/E_0)^{-s}$ .

In quasi-linear models of Fermi II acceleration in isotropic small amplitude Alfvén turbulence (*e.g.* Stawarz & Petrosian (2008)),  $s = \sqrt{9/4 + \epsilon} - 1/2$ , where  $\epsilon = T_{\text{accel}}/T_{\text{escape}}$ . These models include an analogue of scattering from large amplitude magnetic inhomogeneities (Fermi’s original model), in the case where the wave energy spectrum scales in proportion to  $k^{-2}$ , with  $k$  the wavenumber. This case is germane to acceleration due to pair interaction with large scale moving magnetic fluctuations: the acceleration time scale for interaction with large scale moving “eddies” is  $T_{\text{accel}} \approx \lambda_0/c(c/v_{\text{eddy}})^2(B/\delta B)^2 \sim$ , where  $\lambda_0$  is the outer scale of the turbulence, comparable to the shock radius in our case (Camus et al. 2009). The high downstream flow velocity suggests particles escape the turbulence zone through advective loss rather than diffusive escape (at energies much less than a PeV, microscopic diffusion across B, even at the Bohm rate, is negligible compared to the advective losses). Then at flow speed  $\sim c/3$ ,  $T_{\text{escape}} \sim 3R_{\text{shock}}/c$ , leading to  $\epsilon \sim (1/3)(B/\delta B)^2(\lambda_0/R_{\text{shock}})$ . Taking the parameters to be unity yields  $\epsilon \sim 1/3$ , in which case the accelerated spectrum is very hard:  $N(E) \propto E^{-1.3}$  which is similar to the spectrum inferred for the radio emitting pairs in PWNe. Because of the strong radial mixing observed in the MHD models of PWNe, the spectrum created in this turbulent acceleration zone will fill the whole body of the synchrotron emitting nebulae, which provides a natural explanation of the observed

lack of gradients in the radio spectral index of the Crab (Bietenholz 1992). Thus, we revive, in a modern form, the suggestion of Barnes & Scargle (1973), that the wisp motions are responsible for a part of the particle acceleration required to account for PWNe synchrotron emission.

Turning this idea into a full physical model may require extending the MHD models to three dimensions. All models to date have been 2D, axisymmetric, with exclusively toroidal magnetic field. Particles then cannot scatter radially, in order to sample adjacent moving eddies, but are confined to toroidal flux tubes, which move in and out in radius around average positions in the outflow (and inflow, at higher latitudes) in the turbulent region. It is possible that magnetic pumping in these flux tubes might substitute for particle scattering in quasi-isotropic turbulence as an acceleration mechanism (*e.g.*, Melrose (1969); Kuijpers *et al.* (1997)). However, polarization studies already demonstrate that there are substantial poloidal magnetic fields in PWNe inner regions, at least in the Crab. The termination shock instability identified by (Camus *et al.* 2009) is not likely to be restricted to 2D - perhaps the assumption of quasi-isotropic turbulence, with forcing scale  $\sim R_{\text{shock}}$ , is the most natural starting point for further pursuit of this idea.

It is clear that a key point for the model to succeed is that the proposed turbulently accelerated spectrum at low energy merges smoothly into the shock accelerated spectrum at high energy. Since the macroscopic turbulence is closely associated with the shock, a smooth merger is at least thinkable. In this context the meaning of  $\epsilon_c$  changes completely with respect to the Kennel and Coroniti interpretation: this should not be identified with the post-shock temperature (which according to the present model is about an order of magnitude lower), but rather with the energy above which the low energy accelerator (Fermi II in the turbulent flow, in the suggestion made here) fades out and relativistic DSA takes over.

### 7.3 How Do We Move Forward?

Multi-D high resolution MHD and PIC simulations of the termination shock region separating the freely expanding wind from the subsonically expanding nebulae will shed light on the possibly turbulent flow, and on whether that turbulence can act as the low energy accelerator discussed previously. A useful first step would be to couple the diffusion-advection equation in energy space to the MHD calculations. Observationally, infrared observations of the young PWNe, using the Herschel space telescope (Pilbratt 2009) as well as near infrared instruments on the ground and in space, will greatly improve our understanding of the physics behind the broken power laws in energy space inferred here for the injected particle distributions. These instruments will have more than sufficient angular resolution to resolve the PWNe, thus emphasizing the need for multidimensional models to quantitatively interpret the observations.

For all the objects studied, the plasma injection rates, here inferred from the evolutionary models, not simply taken from the average over the nebular lifetimes, exceed  $10^5$  times the Goldreich-Julian rate. Such high rates can be understood only as the result of pair creation within the pulsars' magnetospheres - given the spectral continuity in the SEDs, models which rely on the radio and far-IR emitting parti-

cles, which dominate the injection rates, being accelerated from the thermal plasma in and around the nebulae are less likely than injection from the pulsars. Our results support and extend a long held suspicion (Gallant *et al.* 2002), previously based only on analysis of the Crab Nebula, that the particle loss rates from young, high voltage pulsars are substantially in excess of the inferences of particle *outflow* from all known magnetospheric pair creation models. The answer may lie in intrinsic time dependence of pair creation within pulsar polar caps (*e.g.* Timokhin (2009)), or in the so far unexplored outer magnetosphere accelerators associated with the boundary layer return currents separating the closed and open field lines (Arons 2009). *Fermi* gamma ray observations are and will be useful in constraining magnetospheric pair creation models.

### ACKNOWLEDGMENTS

N.B. was in part supported by NASA through Hubble Fellowship grant HST-HF-01193.01-A, awarded by the Space Telescope Science Institute, which is operated by the Association of Universities for Research in Astronomy, Inc., for NASA, under contract NAS 5-26555; and from NORDITA. JA acknowledges the support of the US National Science Foundation (AST-0507813), the NASA Astrophysics Theory Program (NNG06108G), and the taxpayers of California.

### REFERENCES

- Abdo, A. A., et al. 2010, ApJ, 708, 1254
- Abdo, A. A., et al. 2010, ApJ, 714, 927
- Abdo, A. A., et al. 2009, ApJ, 696, 1084
- Abdo, A. A., et al. 2009, ApJ, 696, 1084
- Albert, J., et al. 2008, ApJ, 700, L127
- Aharonian, F., et al. 2004, A&A, 395, 803
- Aharonian, F., et al. 2004, ApJ, 614, 897
- Aharonian, F., et al. 2005, A&A, 435, L17
- Aharonian, F., et al. 2006, A&A, 456, 245
- Amato, E., Salvati, M., Bandiera, R., Pacini, F., & Woltjer, L. 2000, A&A, 359, 1107
- Amato, E., Guetta, D., & Blasi, P. 2003, A&A, 402, 827
- Amato, E., & Arons, J. 2006, ApJ, 653, 325
- Arons, J. 2009, in 'Neutron Stars and Pulsars', W. Becker, ed., ASSL (Springer: Berlin), 357
- Atoyan, A.M., & Aharonian, F.A. 1996, MNRAS, 278, 525
- Baars, J. W. M. 1972, A&A, 17, 172
- Baldwin, J. E. 1971, The Crab Nebula, 46, 22
- Bandiera, R., Neri, R., & Cesaroni, R. 2002, A&A, 386, 1044
- Barnes, A., & Scargle, J. D. 1973, ApJ, 184, 251
- Becker, R. H., & Helfand, D. J. 1984, ApJ, 283, 154
- Begelman, M. C., & Li, Z.-Y. 1992, ApJ, 397, 187
- Bietenholz, M. F., and Kronberg, P.P. 2004, ApJ, 393, 206
- Bietenholz, M. F., Hester, J., Frail, D., & Bartel, N. 2004, ApJ, 615, 794
- Bietenholz, M. F. 2006, ApJ, 645, 1180
- Blanton, E. L., & Helfand, D. J. 1996, ApJ, 470, 961
- Blondin, J. M., Chevalier, R. A., & Frierson, D. M. 2001, ApJ, 563, 806
- Blumenthal, G. R., & Gould, R. J. 1970, Reviews of Modern Physics, 42, 237

- Bocchino, F., Warwick, R. S., Marty, P., Lumb, D., Becker, W., & Pigot, C. 2001, *A&A*, 369, 1078
- Bock, D. C.-J., & Gaensler, B. M. 2005, *ApJ*, 626, 343
- Bucciantini, N., Blondin, J. M., Del Zanna, L., & Amato, E. 2003, *A&A*, 405, 617
- Bucciantini, N., Bandiera, R., Blondin, J. M., Amato, E., & Del Zanna, L. 2004, *A&A*, 422, 609
- Bucciantini, N., Amato, E., Bandiera, R., Blondin, J. M., & Del Zanna, L. 2004b, *A&A*, 423, 253
- Bucciantini, N. 2008, 40 Years of Pulsars: Millisecond Pulsars, Magnetars and More, 983, 186
- Camus, N., Komissarov, S., Bucciantini, N., & Hughes, P.A. 2009, *MNRAS*, 400, 1241
- Chevalier, R. A. 1982, *ApJ*, 258, 790
- Chevalier, R. A. & Fransson, C. 1992, *ApJ*, 395, 540
- Chevalier, R. A. 2004, *Advances in Space Research*, 33, 456
- Chevalier, R. A. 2005, *ApJ*, 619, 839
- Cheng, K.S. 2007, *ApJ*,
- Collins, B. F., Gotthelf, E. V., & Helfand, D. J. 2002, *Neutron Stars in Supernova Remnants*, 271, 237
- Cox, D. P., Shelton, R. L., Maciejewski, W., Smith, R. K., Plewa, T., Pawl, A., & Różyczka, M. 1999, *ApJ*, 524, 179
- D’Amico, N., et al. 2001, *ApJL*, 552, L45
- DeLaney, T., Gaensler, B. M., Arons, J., & Pivovarov, M. J. 2006, *ApJ*, 640, 929
- Del Zanna, L., Amato, E., & Bucciantini, N. 2004, *A&A*, 421, 1063
- Del Zanna, L., Volpi, D., Amato, E., & Bucciantini, N. 2006, *A&A*, 453, 621
- de Jager, O. C., Ferreira, S. E. S., & Djannati-Ataï, A. 2008, *American Institute of Physics Conference Series*, 1085, 199
- Djannati-Ataï, A., de Jager, O. C., Terrier, R., & et al. 2008, *International Cosmic Ray Conference*, 2, 823
- Du Plessis, I., de Jager, O. C., Buchner, S., Nel, H. I., North, A. R., Raubenheimer, B. C., & van der Walt, D. J. 1995, *ApJ*, 453, 746
- Eisenhauer, F., et al. 2005, *ApJ*, 628, 246
- Forot, M., Hermsen, W., Renaud, M., Laurent, P., Grenier, I., Goret, P., Khelifi, B., & Kuiper, L. 2006, *ApJL*, 651, L45
- Frail, D. A., Giacani, E. B., Goss, W. M., & Dubner, G. 1996, *ApJL*, 464, L165
- Gaensler, B. M., Brazier, K. T. S., Manchester, R. N., Johnston, S., & Green, A. J. 1999, *MNRAS*, 305, 724
- Gaensler, B. M., Arons, J., Kaspi, V. M., Pivovarov, M. J., Kawai, N., & Tamura, K. 2002, *ApJ*, 569, 878
- Gallant, Y., & Arons, J. 1994, *ApJ*, 435, 230
- Gallant, Y., van der Swaluw, E., Kirk, J.G., & Achterberg, A. 2002, in *Neutron Stars in Supernova Remnants*, P.O. Slane and B.M. Gaensler, eds. (San Francisco: ASP Conference Series vol. 271), 99
- Gelfand, J. D., Slane, P. O., & Zhang, W. 2009, *ApJ*, 703, 2051
- Giacani, E. B., Dubner, G. M., Kassim, N. E., Frail, D. A., Goss, W. M., Winkler, P. F., & Williams, B. F. 1997, *AJ*, 113, 1379
- Giuliani, J. L., Jr. 1982, *ApJ*, 256, 624
- Goldreich, P., & Julian, W. 1969, *ApJ*,
- Green, D. A., & Scheuer, P. A. G. 1992, *MNRAS*, 258, 833
- Hamilton, A. J. S., & Sarazin, C. L. 1984, *ApJ*, 281, 682
- Harding, A.K. 2004, personal communication
- Harris, I., Smith, R., Slane, P., Hughes, J. 2006, *Proceedings of the The X-ray Universe 2005* (ESA SP-604), 604, 369
- Helfand, D. J., Collins, B. F., & Gotthelf, E. V. 2003, *ApJ*, 582, 783
- Helfand, D. J., Becker, R. H., White, R. L., Fallon, A., & Tuttle, S. 2006, *AJ*, 131, 2525
- Helfand, D. J. 2007, *Bulletin of the American Astronomical Society*, 38, 114
- Hennesy, G. S., et al. 1992, *ApJL*, 395, L13
- Hester, J. J. 2008, *ARA&A*, 46, 127
- Hester, J. J., et al. 1996, *ApJ*, 456, 225
- Hirschman, J.A., and Arons, J. 2001, *ApJ*, 560, 871
- Hirofani, K., 2008, *ApJ*, 688L, 25
- Horns, D., Aharonian, F., Santangelo, A., Hoffman A.I.D., Masterson C., 2006, *â*, 456, 245
- Hoshino, M., Arons, J., Gallant, Y. A., & Langdon, A. B. 1992, *ApJ*, 390, 454
- Iwamoto, K., et al. 2000, *ApJ*, 534, 660
- Jones, F. C. 1968, *Physical Review*, 167, 1159
- Jun, B.-I. 1998, *ApJ*, 499, 282
- Kalapotharakos, C., & Contopoulos, I. 2009, *â*, 496, 495
- Kargalyshev, O., & Pavlov, G.G. 2008, in “40 Years of Pulsars - Millisecond Pulsars, Magnetars, and More”, C.G. Bassa, Z. Wang, A. Cumming and V.M. Kaspi, eds., *AIP Conf. Proc.*, 983 (New York: Am. Inst. Phys.), 171
- Kardashev, N. 1962, *Soviet Astronomy - AJ*, 6, 317
- Kaspi, V. M., Manchester, R. N., Siegman, B., Johnston, S., & Lyne, A. G. 1994, *ApJL*, 422, L83
- Kennel, C.F., & Coroniti, F.V. 1984a, *ApJ*, 283, 694
- Kennel, C.F., & Coroniti, F.V. 1984b, *ApJ*, 283, 710
- Keshet, U., & Waxman, E. 2005, *Phys. Rev. Lett.*, 94, 111102
- Komissarov, S.S., & Lyubarsky, Y. 2004, *MNRAS*, 349, 779
- Koo, B.-C., & Heiles, C. 1995, *ApJ*, 442, 679
- Kuiper, L., Hermsen, W., Krijger, J. M., Bennett, K., Carrañana, A., Schönfelder, V., Bailes, M., & Manchester, R. N. 1999, *A&A*, 351, 119
- Kuiper, L., Hermsen, W., Cusumano, G., Diehl, R., Schönfelder, V., Strong, A., Bennett, K., & McConnell, M. L. 2001, *A&A*, 378, 918
- Kuijpers, K., Fletcher, L., Abada-Simon, M., Horne, K.D., et al. 1997, *â*, 322, 242
- LaMassa, S. M., Slane, P. O., de Jager, O. C., 2008, *ApJ*, 689L, 121
- Leahy, D. A., & Tian, W. W. 2008, *A&A*, 480, L25
- Livingstone, M. A., Kaspi, V. M., Gotthelf, E. V., & Kuiper, L. 2006, *ApJ*, 647, 1286
- Lyne, A. G., Pritchard, R. S., & Graham-Smith, F. 1993, *MNRAS*, 265, 1003
- MacAlpine, G. M., & Satterfield, T. J. 2008, *AJ*, 136, 2152
- Mazzali, P. A., Iwamoto, K., & Nomoto, K. 2000, *ApJ*, 545, 407
- Mazzali, P. A., et al. 2003, *ApJL*, 599, L95
- Melrose, D. B. 1969, *ApSpSci.*, 4, 165
- Mezger, P. G., Tuffs, R. J., Chini, R., Kreysa, E., & Gemuend, H.-P. 1986, *A&A*, 167, 145
- Morton, T. D., Slane, P., Borkowski, K. J., Reynolds, S. P., Helfand, D. J., Gaensler, B. M., & Hughes, J. P. 2007, *ApJ*, 667, 219
- Murray, S. S., Slane, P. O., Seward, F. D., Ransom, S. M., & Gaensler, B. M. 2002, *ApJ*, 568, 226
- Nakamori, T., et al. 2008, *ApJ*, 677, 297

- Ng, C.-Y., Roberts, M. S. E., & Romani, R. W. 2005, *ApJ*, 627, 904
- Ng, C.-Y., Slane, P. O., Gaensler, B. M., & Hughes, J. P. 2008, *ApJ*, 686, 508
- Ostriker, J. P., & McKee, C. F. 1988, *Reviews of Modern Physics*, 60, 1
- Pacini, F., & Salvati, M. 1973, *ApJ*, 186, 249
- Petre, R., Kuntz, K. D., & Shelton, R. L. 2002, *ApJ*, 579, 404
- Pilbratt, G.L. 2009, in ‘Interstellar Dust from Astronomical Observations to Fundamental Studies’, F. Boulanger, C. Joblin, A. Jones and S. Madden, eds., *EAS Publications Series*, 35, 15
- Rees, M.J., & Gunn, J.E. 1974, *MNRAS*, ,1
- Roberts, M. S. E., Romani, R. W., & Johnston, S. 2001, *ApJL*, 561, L187
- Roberts, M. S. E., Romani, R. W., Johnston, S., & Green, A. J. 1999, *ApJ*, 515, 712
- Rudie, G. C., & Fesen, R. A. 2007, *Revista Mexicana de Astronomia y Astrofisica Conference Series*, 30, 90
- Salter, C. J., Reynolds, S. P., Hogg, D. E., Payne, J. M., & Rhodes, P. J. 1989, *ApJ*, 338, 171
- Shelton, R. L., Cox, D. P., Maciejewski, W., Smith, R. K., Plewa, T., Pawl, A., & Różyczka, M. 1999, *ApJ*, 524, 192
- Spitkovsky, A. 2009, *ApJ*, 698, 1523
- Slane, P. O., Helfand, D. J., & Murray, S. S. 2002, *ApJL*, 571, L45
- Slane, P., Helfand, D. J., van der Swaluw, E., & Murray, S. S. 2004, *ApJ*, 616, 403
- Slane, P., Helfand, D. J., Reynolds, S. P., Gaensler, B. M., Lemiére, A., & Wang, Z. 2008, *ApJL*, 676, L33
- Spitkovsky, A., & Arons, J. 2004, *ApJ*, 603, 669
- Spitkovsky, A. 2006, *ApJ*, 648, L51
- Spitkovsky, A. 2008, *ApJ*, 682, L5
- Stawarz, L., & Petrosian, V. 2008, *ApJ*, 681, 1725
- Stephenson, F. R., & Green, D. A. 2002, *Historical supernovae and their remnants*, by F. Richard Stephenson and David A. Green. *International series in astronomy and astrophysics*, vol. 5. Oxford: Clarendon Press.
- Tanaka, M., et al. 2009, *ApJ*, 692, 1131
- Terrier, R., Lebrun, F., Renaud, M., Bykov, A., & Sturmer, S. 2004, 5th *INTEGRAL* Workshop on the *INTEGRAL* Universe, 552, 501
- Terrier, R., Djannati-Atai, A., Hoppe, S., Marandon, V., Renaud, M., & de Jager, O. 2008, *American Institute of Physics Conference Series*, 1085, 316
- Thompson, D. J., et al. 1996, *ApJSupplements*, 107, 227
- Torii, K., Slane, P. O., Kinugasa, K., Hashimoto, K., & Tsunemi, H. 2000, *Publ. of the Astronomical Society of Japan*, 52, 875
- Truelove, J. K., & McKee, C. F. 1999, *ApJSup.*, 120, 299
- Tsvetkov, D. Y. 2002, *Physics Uspekhi*, 45, 900
- van der Swaluw, E. 2003, *A&A*, 404, 939
- van der Swaluw, E., Achterberg, A., Gallant, Y. A., & Tóth, G. 2001, *A&A*, 380, 309
- van der Swaluw, E., Downes, T. P., & Keegan, R. 2004, *A&A*, 420, 937
- Timokhin, A. 2009, arXiv:0912.5475, to be published in the 2009 Fermi Symposium Conference Proceedings
- Veron-Cetty, M. P., & Woltjer, L. 1993, *A&A*, 270, 370
- Volpi, D., Del Zanna, L., Amato, E., & Bucciantini, N. 2008, *A&A*, 485, 337
- Wolszczan, A., Cordes, J. M., & Dewey, R. J. 1991, *ApJL*, 372, L99